



Contents lists available at ScienceDirect

## Transportation Research Part D

journal homepage: [www.elsevier.com/locate/trd](http://www.elsevier.com/locate/trd)

# Minimizing network-wide emissions by optimal routing through inner-city gating

Deepak Ingle\*, Guilhem Mariotte, Ludovic Leclercq

University Gustave Eiffel, University of Lyon, ENTPE, LICIT, Lyon, France

## ARTICLE INFO

### Keywords:

Traffic emission  
MFD model  
User equilibrium discipline  
Green routing  
Traffic control  
Nonlinear MPC

## ABSTRACT

In this paper, we propose a control and optimization framework to reduce network-wide emissions in an urban traffic network. The framework is comprised of two layers. The first layer (optimal green routing) predicts the optimal splitting coefficients for all Origin–Destination (OD) pairs crossing the city center or bypassing. As implementing optimal routing strategies on the field is almost impossible as we do not have direct control over the user's decisions, we choose to balance travel time through gating at the city perimeter so that the usual Dynamic User Equilibrium (DUE) discipline matches the optimal splitting coefficients. The second layer then adjusts inflows at the city gates to the DUE solution based on the instantaneous travel times corresponding to the optimal routing strategy for each OD pair. The accumulation-based Macroscopic Fundamental Diagram (MFD) model of a single reservoir city with seven arterial routes and six bypass alternatives is developed. A Linear programming problem is formulated to determine the optimal splitting coefficients and a Nonlinear Model Predictive Control (NMPC)-based gating control strategy is designed to track the optimal splitting coefficients. The network-wide emission control framework is compared to three other gating strategies aiming to (i) optimize traffic conditions or (ii) minimize emissions, in the inner-city only, and (iii) optimize traffic conditions in the whole network. A comprehensive analysis conducted on all four approaches is presented. We compare the results of the controlled case with respect to the uncontrolled case and with respect to each other. The comparison results show that: (i) the proposed network-wide emission control strategy significantly outperforms the other two simpler control strategies focusing on inner-city only in reducing the total emission, (ii) but also improves the in total time spent and mean speed at the network-level.

## 1. Introduction

One of the major source of emissions in cities is vehicular traffic which generates harmful gases such as Carbon Monoxide (CO) and Dioxide (CO<sub>2</sub>), Nitrogen Oxides (NO<sub>x</sub>), Hydrocarbon (HC), etc. (Choudhary and Gokhale, 2016; Thaker and Gokhale, 2016; Mascia et al., 2017). The amount of emissions increases during traffic congestion, which also leads to increased fuel consumption. To deal with the problem of congestion and emissions in an urban traffic network, the application of control systems engineering has gained significant attention to the ensure efficient and reliable operation of urban traffic networks. In the following, we concisely discuss such approaches.

\* Corresponding author.

E-mail addresses: [deepak.ingle@univ-eiffel.fr](mailto:deepak.ingle@univ-eiffel.fr) (D. Ingle), [guilhem.mariotte@univ-eiffel.fr](mailto:guilhem.mariotte@univ-eiffel.fr) (G. Mariotte), [ludovic.leclercq@univ-eiffel.fr](mailto:ludovic.leclercq@univ-eiffel.fr) (L. Leclercq).

<https://doi.org/10.1016/j.trd.2020.102411>

In recent years, significant efforts have been made to reduce the congestion by different means like traffic signal optimization, ramp metering, speed control, route guidance, etc. Perimeter control strategies (such as Proportional-Integral-Derivative (PID), Model Predictive Control (MPC), optimal control, etc.) have also been seen as a promising direction to improve network performance e.g., PI controller (Haddad and Shraiber, 2014; Kouvelas et al., 2017a), MPC (Sirmatel and Geroliminis, 2016; Kouvelas et al., 2017b; Yang et al., 2017; Sirmatel and Geroliminis, 2018; Ni and Cassidy, 2019; Kim et al., 2019), etc.

To control the traffic flow, the work in Sirmatel and Geroliminis (2018) and Ding et al. (2017) coupled route guidance with perimeter control to minimize total network delay. This approach proposes a global optimization of the transportation system but assumes that users will comply with optimal route guidance. In practice, users usually prefer to minimize their own cost (travel times) selfishly and have little care for route guidance that do not feel good for them. So, such a strategy is hard to implement in practice. To deal with the waiting queues at the perimeter, work in Hajiahmadi et al., 2015 and Kouvelas et al. (2017a) has derived an optimal perimeter control strategy that accounts for the effect of queuing vehicles. Perimeter control and route guidance strategies for a heterogeneous network (comprised of arterial and freeway) using MPC are discussed in Geroliminis et al. (2013), Haddad et al. (2013), Frejo et al. (2014), Csikós et al. (2018), Han et al. (2018), Yildirimoglu et al. (2018), Ye et al. (2019), Ferrara et al. (2018), and Ye et al. (2019). Hierarchical perimeter control schemes are also been used in the traffic control (see e.g., Fu et al., 2017; Yildirimoglu et al., 2018; Han et al., 2020).

Most of the work in the perimeter control considered the concept of Macroscopic Fundamental Diagram (MFD) to characterize the traffic dynamics in urban networks. This concept provides a well-defined relation between space-mean flow and density. The concept was initially proposed by Godfrey (1969) and similar approaches were introduced later by Mahmassani et al. (1984), Daganzo (2007), Geroliminis and Daganzo (2008).

In the literature, there are two forms of MFD models, the accumulation-based and trip-based model. The accumulation-based model is simply a conservation equation, where the outflow is determined by the MFD function. The trip-based model tracks all vehicle-traveled distances inside the reservoir while assigning the same instantaneous speed to all vehicles defined by MFD. The most recent studies (Mariotte et al., 2017; Mariotte and Leclercq, 2019) showed that the trip-based model provides significant improvements (experienced travel times and the delay between inflow variation to outflow response) in free-flow but the accumulation-based model better deal with solution with saturation and congestion period. As traffic control is operating when traffic conditions are saturated or congested, we choose the accumulation-based formulation here.

Most of the works in this research area focuses on the issues associated with congestion inside the controlled area. The side-effects (such as delays, queues, emissions, etc.) of the perimeter control strategies have received less attention. Side-effects can come from the control strategy itself or from how users adapt to the modified traffic conditions. When perimeter control is active around a control region, two opposite effects can be observed: (i) increased of mean speed inside the region (reduction of congestion), which tend to less emission per kilometer (positive effect) (ii) increase of travel distance for vehicles that choose no longer to enter the region but instead bypass it (negative effect). In recent years, the combination of multi-objective control strategies has been presented but not at the full-city scale. For example, in Groot et al. (2013) the hybrid MPC framework is presented to optimize Total Time Spent (TTS), emissions, and fuel consumption of the freeway traffic. Similarly, several approaches to reduce freeway congestion and emissions is presented, such as a nonlinear optimal control (Pasquale et al., 2015), ramp metering and routing (Pasquale et al., 2017), hybrid MPC (Frejo et al., 2014; Csikós et al., 2018) for signal control, nonlinear MPC (Lin et al., 2013; Jamshidnejad et al., 2017; Chen et al., 2019), etc.

Authors in Luo et al. (2016) have presented a real-time en-route diversion control strategy with multiple objectives (traffic efficiency, emission reduction, and fuel economy) using the MPC framework. The simulation results showed that the routing control can provide a well-balanced network performance but required that users follow diversion guidance. A real-time signal control framework based on a Nonlinear Decision Rule (NDR) for congestion and emission reduction using signal control is presented in Song et al. (2019). Congestion and emissions in traffic networks can also be reduced by road pricing strategies (Cavallaro et al., 2018; Chen and Yang, 2012; Liu and Geroliminis, 2017; Long and Szeto, 2019). If road pricing are known to have positive long-term effect, it may also result in social inequality or unacceptance. Furthermore, pricing to be effective, it should be dynamic and in practice it is difficult to implement fast varying changes in prices. The framework we propose here use the well-established perimeter control framework but in a completely different setting (reduction of network-wide emission). Compared to the pricing schemes, our framework is more reactive and can appropriately balance Origin–Destination (OD) flows within the different route options in real-time.

In this paper, we directly reproduce traffic conditions at the full-city level considering three main network components (inner-city, inbound links, and bypass network). To access the traffic-related emissions, we need to use appropriate emission laws, i.e., macroscopic ones. Macroscopic models use mainly mean speed and travel distance to estimate network-wide emission levels. Several macroscopic emission models exists, e.g., Mobile Source Emission Model (MOBILE) (EPA, 2003), Emission Factors (EMFAC) model (CARB, 2017) and COPERT IV model (Ntziachristos et al., 2009), Handbook Emission Factors for Road Transport (HBEFA) (Keller, 2017), etc. For the review and comparison of the above emission models, refer to Fujita et al. (2012), Franco et al. (2013), Osorio and Nanduri (2015), Wang et al. (2018).

Note that, authors in Shabihkhani and Gonzales (2014) used the MFD to analytically estimate the network-wide emission and compared it to the microscopic emission model presented in EPA (2014). A framework for modeling the traffic emissions with the Network Fundamental Diagram (NFD) concept is presented in Csikós et al. (2015) and the model accuracy is compared with the VERSIT + Micro model. The results of two case studies showed that the macroscopic model (based on mean speed and COPERT IV) leads to the good estimates for emissions. Authors in Saeedi et al. (2018) proposed a mesoscopic approach that is capable of estimating emission for large networks, as well as capturing the effects of traffic flow dynamics. In this study, they used the network-wide traffic flow characteristics from NFD in the estimation of vehicular emissions. The mean speed-based emission models have been used to

estimate fuel consumption (Samaras et al., 2019). These aforementioned works showed that the mean speed and travel distance obtained from MFD/NFD models are accurate enough to predict good estimations when using macroscopic emission laws.

Our review of the different strategies to reduce traffic emission shows that, optimal routing is very promising because it switches some vehicles from the shortest paths with usually higher congestion to a longer paths with higher speed. This can reduce the emissions despite the increase of trip length. Unfortunately, such strategies are almost impossible to implement in practice as users can easily assess their travel time increase and decide not to follow the guidance. Contrary to railways or air traffic, no central control authority can adequately enforce vehicle routing in the road network. This is why we propose here to investigate a completely new concept corresponding to an indirect control strategy that can result in optimal and green routing. The idea is to detour the classical objective of perimeter/gating strategy, i.e., imposing the traffic condition inside the controlled area, to enforce delays to enter the region when re-routing vehicles would be more effective for reducing the total emission. In a sense, we introduce special costs in terms of travel times to lure the rooted user equilibrium discipline in a favorable way for the environment, gating queues will force user re-routing when necessary.

In short, our network-wide emission control strategy is composed of two layers. The first layer (optimal green routing) determines for the next time horizon the optimal splitting coefficient for all OD pairs (only two alternatives are possible for each OD). The second layer is a Nonlinear Model Predictive Control (NMPC)-based gating controller, which determines the flow limits that can enter the city at each time-step over the time horizon so that the DUE discipline distributes users among both alternatives as close as possible to the optimal splitting coefficient. The efficiency of the proposed strategy is demonstrated through a case study of a single reservoir city (with one internal route, six OD pairs, and six bypass routes) and its performance is analyzed and compared with the nocontrol case. The performance of the network-wide emission control strategy is presented and compared with the congestion and emission control only inside the reservoir. In all cases, NMPC results are compared with the no-control case. Results indicate that, the proposed strategy can significantly reduce network-wide emissions and TTS, and increase mean speed in the reservoir.

This work is a continuation and extension of our earlier work (Ingole et al., 2019) where we first presented the concept of network-wide emission mitigation based on optimal gating. This paper presents all the methodological details and more complex implementation with different network settings. We improved, in particular, the smoothing of optimal emission coefficients and present a test case where multiple gates are acting simultaneously. Finally, we present a full comparison with other classical gating control approaches. This paper also benefits from some earlier methodological contributions from Ingole et al. (2020). This paper presents a methodological framework to predict user's re-routing attitudes when the perimeter flow of a region is controlled. This framework calculates the fraction of vehicles that take a detour instead of crossing the inner city to fulfill user equilibrium conditions, i.e., the same travel times for all alternatives. In Ingole et al. (2020), the perimeter control strategy is classical and only minimizes the total travel distance inside the region. We used a simple PI controller that monitors the deviation between the current and optimal accumulation inside the inner city. We showed that it could lead to undesirable side effects, like a significant increase in total network emissions because of the extra distances traveled by some vehicles. This inspires the current paper, where we present a completely new control framework able to find the right balance between the detour and the traffic conditions inside the inner city. The challenge from a control point of view is that we decided not to directly manipulate the path flow between the different alternatives for each OD pairs because this is not feasible in practice. We instead chose to keep the field-proven perimeter control framework and indirectly modified the flow distributions by controlling the inner-city entry gates. To this end, we propose here a double-layer optimization framework. The upper-level derives an optimal routing strategy from a linear optimization problem using quasi-static approximations of the system dynamics. The lower-level makes the system converges to the optimal path flow distributions using an advanced predictive control framework (NMPC) that considers the full system dynamics.

The rest of the paper is organized as follows. The urban network under consideration is introduced in the next section. Section 2 describes the problem statement of this work. In Section 3, an overview of the traffic flow model is given. Section 4 describes the routing strategy and emission calculations. Section 5 describes the design of the gating control strategy. Section 6 demonstrates the results of the proposed approach and the concluding remarks are given in Section 7.

## 2. Problem statement

The city network is partitioned into two parts: the inner-city, which is inside the control perimeter and the suburb network. We consider three main OD points outside the city North, Southeast, and Southwest. The proposed modeling framework can adjust to any number of OD points and we choose three to keep the result analysis tractable. For each OD pair (six in total), users can choose to either take the shortest path in distance and cross the city or make a detour and bypass the center through the suburb network. We introduce then the concept of regional paths, which is widely used for MFD simulations. The regional paths aggregate a list of local paths on the real-network with the same origin and destination into one. Thus, for the six OD pairs, two regional paths are considered heading to the definition of six regional paths inside the city and six others around in the suburbs, see Fig. 1. Note that all internal regional paths (in the city) are preceded by an Inbound Link (IL) just upstream of the gating points. It represents the aggregation of all portions of the road on which vehicles may wait due to inflow limitation (natural propagation of congestion or control actions). Finally, a supplementary internal route is added to represent vehicles that only travel inside the inner-city.

We assume that the traffic dynamics of the reservoir is given by a well-defined production-MFD  $P(n)$  (in [veh·m/s]), or equivalently, a speed-MFD  $V(n)$  (in [m/s]), where  $n$  (in [veh]) is the total number of vehicles in the reservoir. The  $P(n)$  is characterized by values such as: jam accumulation  $n_j$ , critical accumulation  $n_c$ , maximum production or capacity  $P_c = P(n_c)$ , and free-flow speed  $\tilde{v} = dP(0)/dn$ . The entry and exit of the reservoir gather all their respective individual nodes. At the entry, total effective inflow is given by  $q_{in}(t)$  and at the exit, total effective outflow is given by  $q_{out}(t)$  (in [veh/s]).

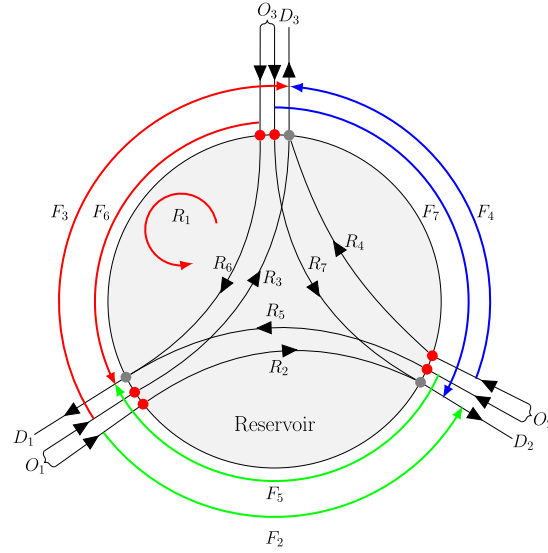


**Fig. 1.** Single reservoir network with one internal route ( $R_1$ ), six external routes ( $R_2, \dots, R_7$ ), six bypass routes ( $F_2, \dots, F_7$ ), and six inflow controlled gates.

The objective of this work is threefold: first, to develop an accumulation-based model and DUE model for the network shown in Fig. 1; second, to design a model-based gating control strategy to reduce network-wide  $\text{NO}_x$  emission, and the third is to compare the performance of our network-wide emission control strategy with the classical NMPC controller targeting inner-city only. Note that only  $\text{NO}_x$  emission is considered to demonstrate our framework but as all emissions curves have similar trends concerning mean speed, all the methodology can be generalized for other pollutants. Only numerical results will be changed. It is also worth to mention that in Layer 1, we use only  $\text{NO}_x$  to find optimal green routing.

### 3. Traffic modeling

In this section, we introduce the accumulation-based MFD model designed for a single reservoir with multiple routes. The total system includes, regional routes inside the city network and bypass routes in the suburbs. First, we ignore the bypass and inbound links and focus on the traffic dynamics inside the reservoir. The accumulation-based model considering multiple internal routes  $\mathcal{R}$  of lengths  $L_i$  has been extensively studied in Mariotte and Leclercq (2019). The accumulations  $n_i$  are the numbers of vehicles traveling on each route  $i$  inside the reservoir, satisfying the following system (Geroliminis, 2015):

$$\frac{dn_i}{dt} = q_{\text{in},i}(t) - q_{\text{out},i}(t), \quad \forall i \in \{1, \dots, c, \mathcal{R}\}, \quad (1)$$

where  $q_{\text{in},i}(t)$  is the effective inflow and  $q_{\text{out},i}(t)$  is the outflow of route  $i$ .

In this work, we use the model of flow exchange at perimeter proposed by Mariotte and Leclercq (2019) to define  $q_{\text{in},i}(t)$  and  $q_{\text{out},i}(t)$ . The effective inflow  $q_{\text{in},i}(t)$  for transfer trip  $i$  is the result of rivalry between the corresponding demand  $\lambda_i(t)$  and entry supply function  $I_i(n_i, n)$ . We also account for a queue at the entry of each route (described by a point-queue model) to store the waiting vehicles when the demand is not satisfied. These vehicles are physically waiting on the corresponding inbound link in our network. The inflow of internal trips is assumed to be unrestricted, thus equal to its demand. As a result, the inflow of any route  $i$  is expressed by:

$$q_{\text{in},i}(t) = \begin{cases} \min(\lambda_i(t), I_i(n_i(t), n(t)), u_i(t)), & \forall i \geq 2, \\ \lambda_i(t), & i = 1, \end{cases} \quad (2)$$

where  $u_i(t)$  is the gating inflow obtained by perimeter controller and the entry supply function is given by:

$$I_i(n_i, n) = \begin{cases} \frac{n_i}{n} \frac{P_c}{L_i}, & \text{if } n < n_c, \\ \frac{n_i}{n} \frac{P(n)}{L_i}, & \text{otherwise.} \end{cases} \quad (3)$$

This shape is however too restrictive because it does not allow the inflow values to exceed the reservoir flow capacity by construction. If this was true, there would be no need for controlling inflows during congestion. In reality, the entry flow is at first limited by the total capacity of entry points, which is higher than the reservoir capacity. To mimic this effect, we added a fixed coefficient  $\alpha > 1$  to let the total inflow temporarily exceed the reservoir capacity. In this work, we fixed  $\alpha = 1.3$ , see Fig. 2.

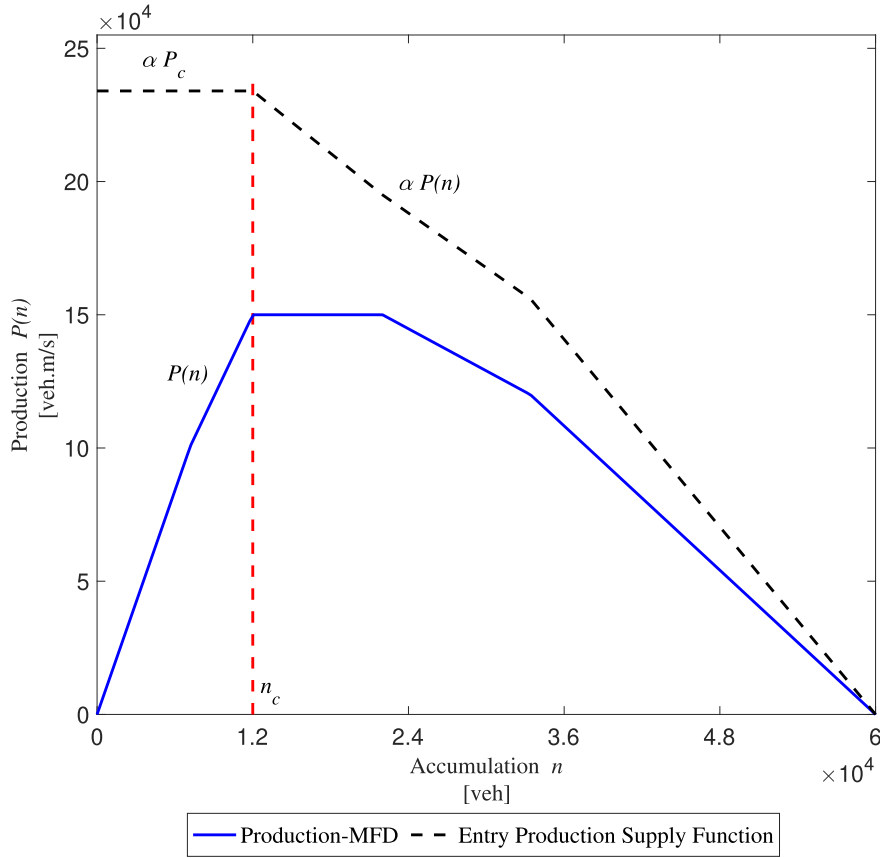


Fig. 2. Production-MFD and production entry supply function.

The outflows  $q_{out,i}(t)$  are the result of reservoir inner dynamics and inter-dependent through the following relationships between the most constrained outflow  $j$  and other effective outflow  $i$  as follows (Mariotte and Leclercq, 2019):

$$q_{out,j}(t) = \min(\mu_j(t), O_j(n_j, n)), \quad (4)$$

where  $j = \operatorname{argmin}_{1 \leq i \leq R} \frac{\mu_i}{O_i(n_i, n)}$  and

$$q_{out,i}(t) = \frac{n_i(t)}{n_j(t)} \frac{L_j}{L_i} q_{out,j}(t), \quad \forall i \neq j. \quad (5)$$

The function  $O_i(n_i, n)$  is the demand for outflow of route  $i$ . As in (Mariotte and Leclercq, 2019), in over-saturated situations, we assume this demand to be maximum for transfer trips (outflow at the reservoir exit border), and to decrease along the production-MFD for internal trips (the rate at which destinations are reached inside the reservoir): for a transfer trip:

$$O_i(n_i, n) = \begin{cases} \frac{n_i}{n} \frac{P(n)}{L_i}, & \text{if } n < n_c, \\ \frac{n_i}{n} \frac{P_c}{L_i}, & \text{otherwise,} \end{cases} \quad (6)$$

for an internal trip:

$$O_i(n_i, n) = \frac{n_i}{n} \frac{P(n)}{L_i}. \quad (7)$$

For more details about the considered accumulation-based model, see Mariotte et al. (2017), Mariotte and Leclercq (2019).

## 4. Routing Discipline and Emission Calculations

### 4.1. User equilibrium discipline

For each OD pairs, as shown in Fig. 1, the users willing to enter the route  $R_i$  ( $i \geq 2$ ) can choose to take the bypass  $F_i$  instead of entering the inbound link and crossing the reservoir to reach their destination. The bypass  $F_i$  is assumed to have a higher capacity

than all the city street represented by route  $R_i$ , so that the travel times on the suburb route is almost constant. Note that this modeling framework has been extended with time-dependent travel times profiles for bypass routes as long as the profile is piece-wise constant and time intervals are not too small (Ingole et al., 2020). We keep here a single mean travel time value for each suburb route as this is not essential to demonstrate the capabilities of our global framework to minimize emissions. Hence, if we assume that these travelers are making their choices according to DUE, we should have the following relationships in travel time at any time  $t$ :

$$\begin{cases} T_{IL,i}(t) + T_{R,i}(t + T_{IL,i}(t)) < T_{F,i} & \Leftrightarrow \text{no one chooses the bypass,} \\ T_{IL,i}(t) + T_{R,i}(t + T_{IL,i}(t)) = T_{F,i} & \Leftrightarrow \text{at least one user chooses the bypass,} \end{cases} \quad (8)$$

where  $T_{F,i}$  is the bypass constant travel time,  $T_{IL,i}(t)$  and  $T_{R,i}(t)$  are the instantaneous travel times on the inbound link and in the reservoir, respectively, for route  $R_i$  (that will be experienced by users entering the reservoir or the inbound link at  $t$ ). The inbound link is assumed to have a total length  $L_{IL,i}$ , and to consist of two parts: the first one is free-flow with speed  $\tilde{v}_{IL,i}$ , and the second one is congested, dynamically represented by a point-queue model. Thus, its travel time consists of two terms:  $T_{IL,i}(t) = L_{IL,i}/\tilde{v}_{IL,i} + \delta_{IL,i}(t + L_{IL,i}/\tilde{v}_{IL,i})$ , where  $\delta_{IL,i}(t)$  is the exact predictive delay in the inbound link (that will be experienced by users willing to enter the reservoir at  $t$ ).

Both  $\delta_{IL,i}(t)$  and  $T_{R,i}(t)$  are the result of traffic dynamics that will be observed inside the reservoir after  $t$ . During the simulation, because we do not know the future evolution of the system at  $t$ , we choose to estimate these values based on the current state observation:

$$T_{R,i}^*(t) = L_i/V(n(t)), \quad (9)$$

$$\delta_{IL,i}^*(t) = n_{IL,i}(t)/q_{out,IL,i}(t - dt), \quad (10)$$

where  $n_{IL,i}(t)$  is the accumulation and  $q_{out,IL,i}(t - dt) = q_{in,i}(t - dt)$  is the effective outflow of the inbound link  $i$ , estimated from the previous time step  $t - dt$  as we do not know it at  $t$ . Then, the estimation  $T_{IL,i}^*(t)$  of the inbound link predictive travel time is directly obtained with  $\delta_{IL,i}^*(t)$  as  $T_{IL,i}^*(t) = L_{IL,i}/\tilde{v}_{IL,i}(t) + \delta_{IL,i}^*(t)$ .

For given route  $i$ , switching the users to the bypass  $F_i$  is achieved by splitting the inflow demand  $\lambda_i(t)$  into the inbound link inflow  $q_{in,IL,i}(t)$  and the bypass inflow  $q_{in,F,i}(t)$  according to the following model:

**Case 1** If  $T_{IL,i}^*(t) + T_{R,i}^*(t) < T_{F,i}$ , users switch to the reservoir route:

$$\chi_i(t) = (1 - b_i)q_{in,F,i}(t - dt)/\lambda_i(t - dt), \quad (11a)$$

$$q_{in,IL,i}(t) = (1 - \chi_i(t))\lambda_i(t), \quad (11b)$$

$$q_{in,F,i}(t) = \chi_i(t)\lambda_i(t). \quad (11c)$$

**Case 2** Otherwise, users switch to the bypass:

$$\chi_i(t) = (1 - b_i)q_{in,F,i}(t - dt)/\lambda_i(t - dt) + b_i, \quad (12a)$$

$$q_{in,IL,i}(t) = \max((1 - \chi_i(t))\lambda_i(t); q_{in,IL,i}^{\min}), \quad (12b)$$

$$q_{in,F,i}(t) = \lambda_i(t) - q_{in,IL,i}(t). \quad (12c)$$

The inflow splitting coefficient  $\chi_i(t) \in [0, 1]$  corresponds to the proportion of users on path  $i$  who just took the bypass alternative  $F_i$  to reach their destination. The calculation of this coefficient is smoothed via (11a) and (12a), which represents the progressive adaptation of the users to the instantaneous modification of the estimated travel times. The smoothing coefficients  $b_i$  are in  $[0,1]$ , the application of UE discipline is quite instantaneous when the  $b_i$  are chosen close to 1.

Then, the accumulation in each inbound link  $i$  is governed by the following conservation equation:

$$\frac{dn_{IL,i}}{dt} = q_{in,IL,i}(t) - q_{out,IL,i}(t), \quad (13)$$

where the outflow is equal to the inflow in route  $i$ , i.e.,  $q_{out,IL,i}(t) = q_{in,i}(t)$ . On the other hand, traffic dynamics in the bypass is considered to be always constant travel time, thus represented by the following conservation equation with a fixed delay (the bypass free-flow travel time  $T_{F,i}$ ):

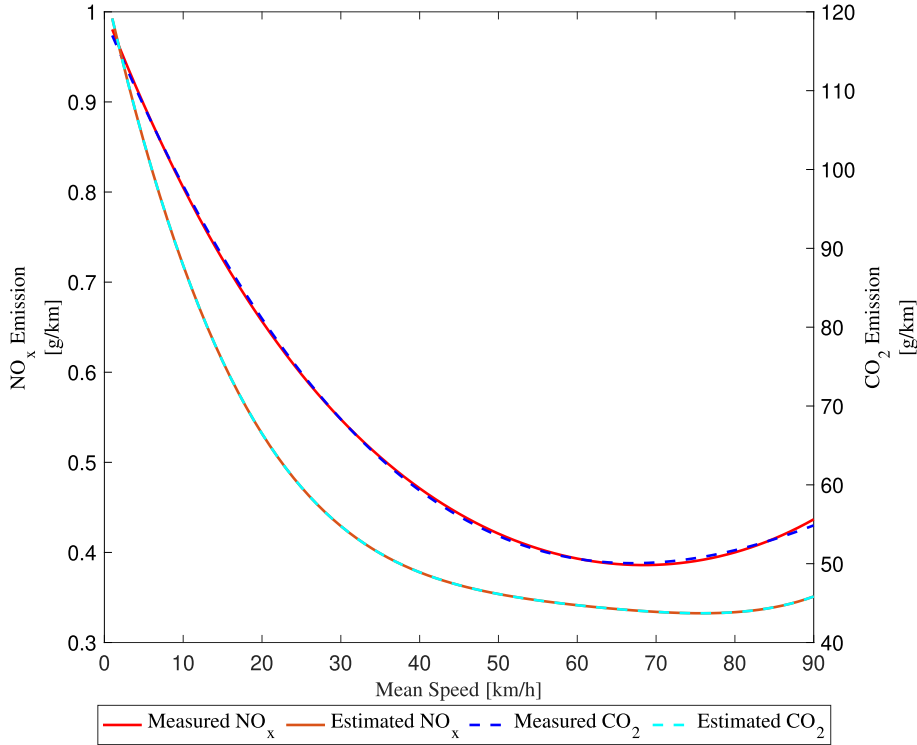


**Fig. 3.** NO<sub>x</sub> and CO<sub>2</sub> emissions for passenger cars taken from COPERT IV model (Ntziachristos et al., 2009) and estimated curve represents the curve obtained after applying curve fitting technique to relate mean speed with .emission factor.

$$\frac{dn_{F,i}}{dt} = q_{in,F,i}(t) - q_{in,F,i}(t - T_{F,i}). \quad (14)$$

#### 4.2. Emission model

Vehicle emissions can be obtained by emission models. Here, we use macroscopic emission rules that provide the emission rate (in [g/km]) of a reference vehicle depending on the mean speed  $v^*(t)$ . These rules come from the COPERT IV framework (Ntziachristos et al., 2009) and have been integrated with the fourth-degree polynomial for simplicity (Lejri et al., 2018). In this work, we obtained the Emission Factor (EF) model of (NO<sub>x</sub>) and (CO<sub>2</sub>) from COPERT IV based on the reference emission data recorded for the mean speed ( $v^*$ ) profile of personal cars. Then, the evolution of the emission level  $E_{dt}(t)$  (in [g]) of one pollutant between  $t$  and  $t + dt$  is calculated as:

$$E_{dt}(t) = EF(v^*(t)) \times n^*(t) \times v^*(t) \times dt, \quad (15)$$

where  $EF(v^*(t))$  is the emission factor of the pollutant considered (in [g/km]),  $n^*(t)$  the accumulation and  $v^*(t)$  the mean speed at  $t$ . The emission factor  $EF(v^*)$  is estimated through curve fitting technique applied to emission curves shown in Fig. 3.  $E_{dt}(t)$  corresponds to instantaneous emissions because it is calculated for a small-time step,  $dt = 1$  s. On route  $i$  in the reservoir,  $n^*(t)$  is the partial accumulation  $n_i(t)$ , and  $v^*(t)$  is the reservoir mean speed  $v(t)$ . In the IL for route  $i$ ,  $n^*(t)$  is the link accumulation  $n_{IL,i}(t)$ , and  $v^*(t)$  is the link mean speed  $v_{IL,i}(t)$ . On the bypass,  $n^*(t)$  is the bypass accumulation  $n_F(t)$ , and  $v^*(t)$  is the bypass free-flow speed  $\tilde{v}_F$ . The mean speed in inbound link  $i$  is obtained as:

$$v_{IL,i}(t) = \frac{L_{IL,i}}{T_{IL,i}(t)}, \quad (16)$$

where  $L_{IL,i}$  and  $T_{IL,i}$  are respectively the inbound link length and travel time.

#### 4.3. Layer 1: optimal green routing

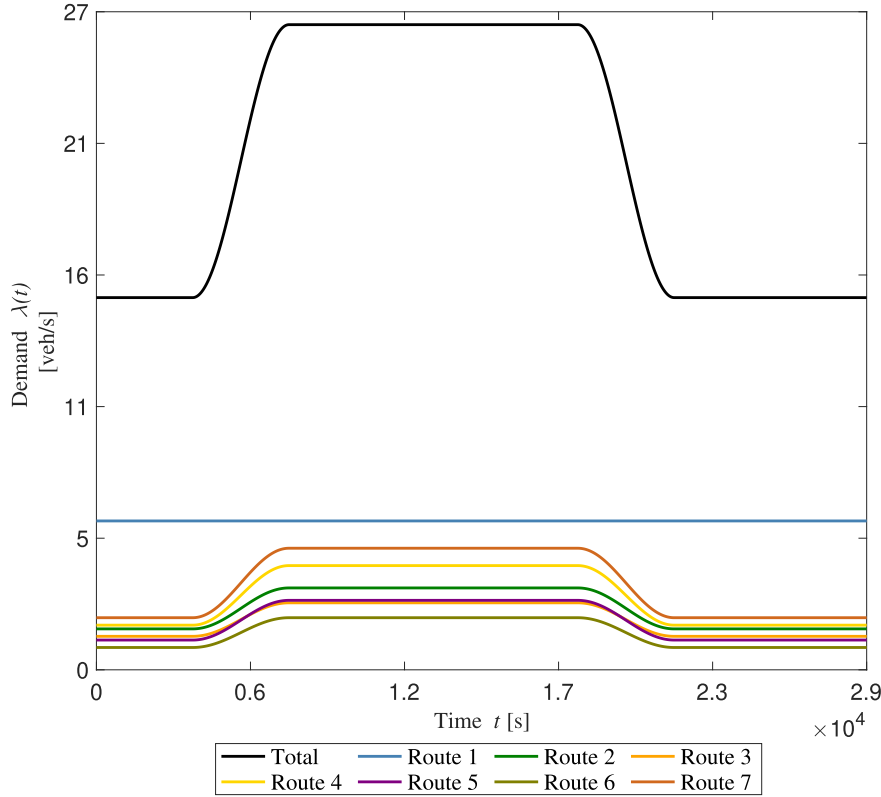
As explained in the introduction, it is difficult to enforce optimal green route guidance when users are free to choose their route and often favor the shortest path in time. So, users usually comply with DUE discipline as discussed in Section 4.1. So, we are going first to calculate what would be the optimal split between the central and suburbs routes for all OD pairs (layer 1) and then make users comply with this by modifying the travel time on the central routes through gating. Note that the gating can only work if users



**Table 1**

Values of the MFD model parameters used in the case study. All bypasses and the inbound links have the same characteristics.

Parameter	Value	Unit
Reservoir trip lengths ( $L_i$ )	$[5 \ 6 \ 8.5 \ 5.5 \ 8 \ 7.5 \ 8.5] \times 10^3$	m
Reservoir maximum production ( $P_c$ )	150000	veh.m/s
Reservoir free-flow speed ( $\tilde{v}$ )	14	m/s
Reservoir jam accumulation ( $n_j$ )	60000	veh
Reservoir critical accumulation ( $n_c$ )	12000	veh
Bypass trip length ( $L_{F,i}$ )	$[19.5 \ 22.5 \ 22.5 \ 22.5 \ 19.5 \ 22.5] \times 10^3$	m
Bypass free-flow speed ( $\tilde{v}_F$ )	14	m/s
Bypass free-flow travel time ( $T_{F,i}$ )	$[1250 \ 1428 \ 1428 \ 1428 \ 1250 \ 1428]$	s
Inbound link free-flow speeds ( $\tilde{v}_{IL,i}$ )	19	m/s
Inbound link trip lengths ( $L_{IL,i}$ )	$[2.5 \ 2.5 \ 2.5 \ 2.5 \ 2.5 \ 2.5] \times 10^3$	m

**Fig. 4.** Traffic inflow demand profiles for all routes and its total.

would be likely to enter the city while they should have taken the detour to minimize emission. This happens when the speed on the central routes is low and when the extra emissions related to congestion exceed the extra emission generated by the extra distance through the detour. So, we know in advance that the gating strategy will not match all time the optimal green routing strategy but at least it would tend to it when possible.

In our proposed framework we consider two layers. The first layer is to determine the optimal green routing to minimize network-wide emission. Here, we use only  $\text{NO}_x$  to find optimal green routing. Let us assume the variable  $\beta_i^r(t) \in [0, 1]$  as the optimal coefficient for each bypass route,  $F_i$  and  $(1 - \beta_i^r(t))$  for each regional route,  $R_i$  and inbound link,  $IL_i$ .  $\beta_i^r(t)$  gives the optimal proportion of users who should go to the bypass at  $t$ . So, in total, we will have six optimal coefficients  $\beta_i^r(t) \in [0, 1] \quad i = 2, \dots, 7$ . Now, the objective is to find the values of  $\beta_i^r(t)$  which minimize network-wide emission for known demand profile ( $\lambda(t)$ ) and a fixed time horizon. For this, we solve the Linear Programming (LP) problem to estimate optimal  $\beta_i^r(t)$  that minimizes the Total Emission ( $E_\tau$ ) for a predefined time horizon of  $\tau = 60$  s. To calculate the emissions at each  $\tau$ , we assume the fixed accumulation and speed (equal to the values at  $t$ ) for  $[t, t + \tau]$ . The predicted  $E_\tau$  for each simulation time step between  $[t, t + \tau]$  is calculated as follows:

$$E_{\tau,F}(t) = EF(\tilde{v}_F(t)) \times \lambda_i(t) \times \tau \times L_{F,i}, \quad (17a)$$



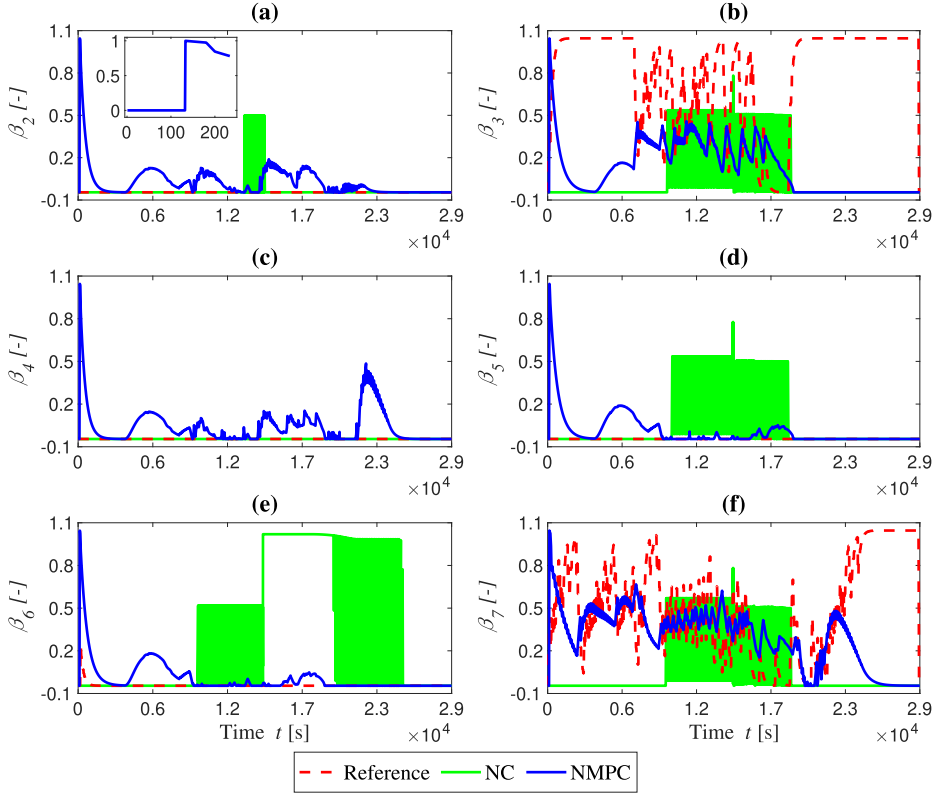


Fig. 5. Performance evaluation of  $\beta_i(t)$  coefficient for nocontrol and network-wide NMPC.

$$E_{\tau, \text{res.}}(t) = EF(v(t)) \times \lambda_i(t) \times \tau \times L_i, \quad (17b)$$

$$E_{\tau, \text{IL}}(t) = EF(v_{\text{IL},i}(t)) \times \lambda_i(t) \times \tau \times L_{\text{IL},i}. \quad (17c)$$

Combining (17a)-(17c) and considering optimal splitting coefficient, we get the total emission in the network as:

$$E_{\tau}(t) = E_{\tau, F}(t)\beta_i^r(t) + (E_{\tau, \text{res.}}(t) + E_{\tau, \text{IL}}(t))(1 - \beta_i^r(t)). \quad (18a)$$

To find the optimal splitting coefficient  $\beta_i^r(t)$  at each time step  $t$  an LP problem is formulated as:

$$\min_{\beta_i^r(t)} E_{\tau, F}(t)\beta_i^r(t) + (E_{\tau, \text{res.}}(t) + E_{\tau, \text{IL}}(t))(1 - \beta_i^r(t)), \quad (19a)$$

$$\text{s. t. } 0 \leq \beta_i^r(t) \leq 1, \quad \forall t \in [t, t + \tau]. \quad (19b)$$

After obtaining the  $\beta_i^r(t)$  values for all time step between  $[t, t + \tau]$ , we apply a simple filtering technique corresponding to the moving average as follows:

$$\beta_i^r(t) = \frac{1}{4}(\beta_i^r(t) + 2\beta_i^r(t - dt) + \beta_i^r(t - 2dt)). \quad (20)$$

The obtained  $\beta_i^r(t)$  values are now considered as the reference for the perimeter gating control strategy in layer 2 for each time step  $t$  over the time horizon  $[t, t + \tau]$ .

The values of controlled variable  $\beta_i(t)$  in the simulator were estimated at the exit of the reservoir based on the outflow observation as:

$$\beta_i(t) = 1 - (q_{\text{out},i}(t - dt)/\lambda_i(t - dt)). \quad (21)$$

Note that it is straightforward to transform (19) into an objective function that minimize total time spent at the network-level, this will be explore in Section 6.2.3.

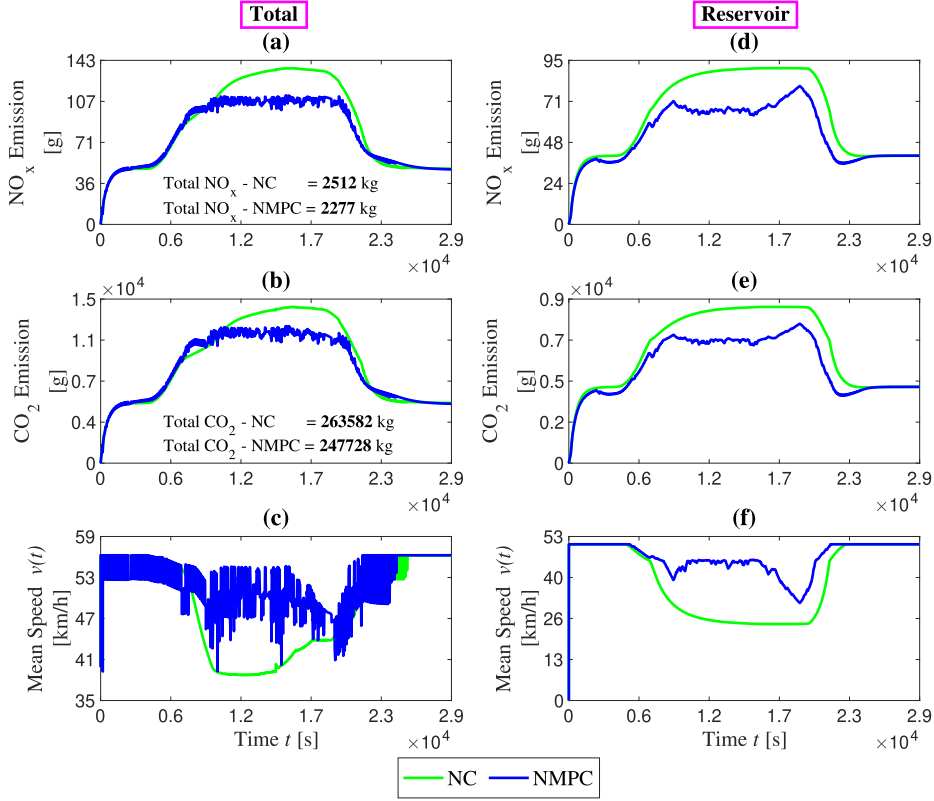


**Fig. 6.** Performance evaluations of network-wide emissions and mean speed (left column) and reservoir emission and mean speed (right column) for nocontrol and network-wide NMPC.

## 5. Layer 2: nonlinear model predictive control as a gating strategy

### 5.1. Concept

Nonlinear MPC is a well-known family of control algorithms used for designing and implementing feedback control systems. MPC provides an effective and general means to design control systems for nonlinear multivariable systems with operating constraints on input and output variables. In the MPC algorithm, the control action is obtained by solving a Constrained Finite-Time Optimal Control (CFTOC) problem for the current state of the plant at each sampling time. The sequence of optimal control inputs is computed for a predicted evolution of the system model over a finite-time horizon. However, only the first element of the control sequence is applied, and the state of the system is then measured again at the next sampling time. This so-called Receding Horizon Controller (RHC) introduces feedback to the system, thereby allowing for compensation of potential modeling errors or disturbances acting on the system (Borrelli et al., 2017; Grüne and Pannek, 2017; Mayne, 2014).

### 5.2. Problem formulation for emission control

NMPC as a CFTOC problem (in discrete-time) for reference (network-wide emission) tracking is represented as follows:

$$\min_{u_0, \dots, u_{N-1}} \sum_{k=0}^{N-1} (\|y_k - y_{\text{ref},k}\|_Q^2 + \|\Delta u_k\|_R^2), \quad (22a)$$

$$\text{s. t.} \\ x_{k+1} = f(x_k, u_k), \forall k \in \{0, \dots, N-1\}, \quad (22b)$$

$$y_k = g(x_k, u_k), \forall k \in \{0, \dots, N-1\}, \quad (22c)$$

$$\Delta u_k = u_k - u_{k-1}, \forall k \in \{0, \dots, N-1\}, \quad (22d)$$

$$u_{\min} \leq u_k \leq u_{\max}, \forall k \in \{0, \dots, N-1\}, \quad (22e)$$

$$u_{-1} = u(t - T_s), \quad (22f)$$

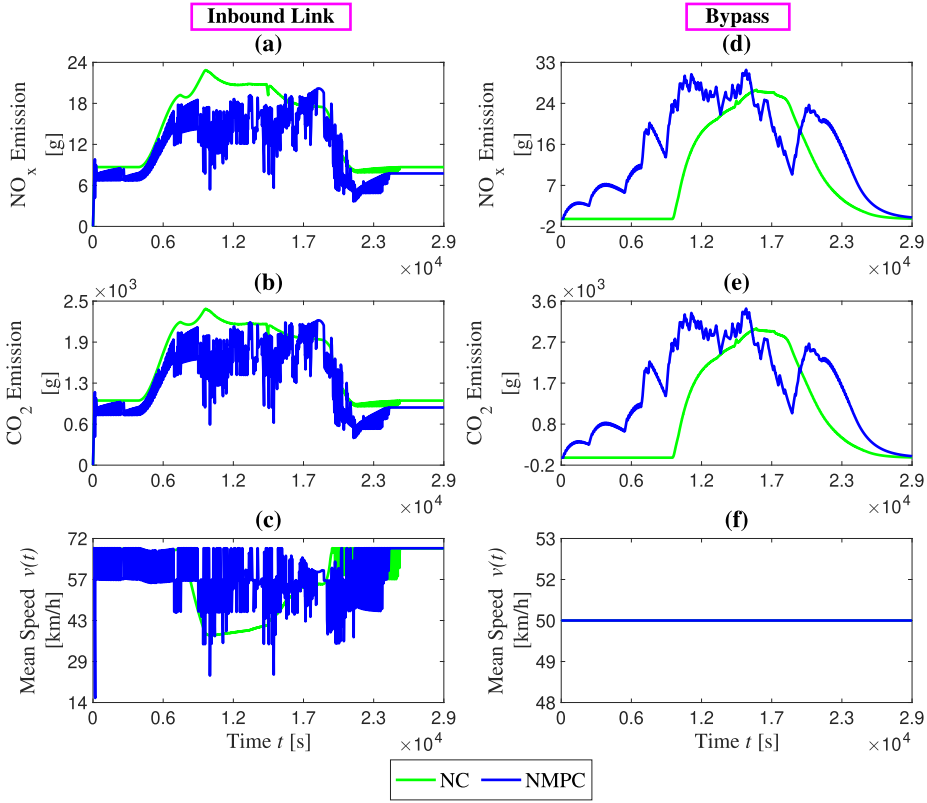


**Fig. 7.** Response of inbound link emissions and mean speed (left column) and bypass emissions and mean speed (right column) for nocontrol and network-wide NMPC.

$$x_0 = x(t), \quad (22g)$$

where  $x \in \mathbb{R}^{n_x}$ ,  $y \in \mathbb{R}^{n_y}$ , and  $u \in \mathbb{R}^{n_u}$  are the vector of state, output, and input, respectively at time  $t_k$ , for time index  $k$ . In (22a),  $y_{\text{ref}}$  corresponds to the reference values of the splitting coefficients  $\beta_i^r(t)$  (from layer 1 by (20)) and  $y$  corresponds to the outputs corresponding to splitting coefficient  $\beta_i(t)$  obtained from (21). Here, we consider NMPC with  $\Delta u$  formulation in order to prevent oscillations and frequent shifting in the control actions and reduce steady state error (see Zegeye et al., 2009, Baskar et al., 2012, Li et al., 2019).

We denote  $N$  as the prediction horizon and  $T_s$  as sampling time of the plant. The cost function is weighted by  $Q \geq 0$  and  $R > 0$ . The function  $f$  in (22b) describes the nonlinear dynamics of the traffic network under consideration which is as given by (1). The evolution of the output  $y_k$  is given by the function  $g$  according to (22c). The function  $f: \mathbb{R}^{n_x} \times \mathbb{R} \rightarrow \mathbb{R}^{n_x}$  is locally Lipschitz continuous and  $g: \mathbb{R}^{n_x} \rightarrow \mathbb{R}^{n_y}$  is continuous. The optimization is accomplished with respect to  $u_0, \dots, u_{N-1}$ . Following the concept of a receding horizon control, only the first optimized input, i.e.,  $u_0^*$  is implemented to the system in (1). The whole procedure is then repeated at a next sampling time with newly measured initial conditions in (22g).

The direct solution of the continuous-time CFTOC problem (22) comprised of two steps: integration, i.e., solving the Ordinary Differential Equation (ODE) and solving a nonlinear optimization problem. The second task is computationally-complex, which needs fast Nonlinear Programming (NLP) solvers and powerful hardware. Compounding this difficulty is the real-time aspects of NMPC, where a result must be ready within one sample time.

### 5.3. Implementation

The proposed two-layered framework based on optimal routing and NMPC perimeter gating strategy with the MFD model were implemented and synthesized in a MATLAB. The NMPC objective function is to reduce network-wide emission via optimal splitting coefficients  $\beta_i(t)$  while minimizing the traffic flow at the six gates of the perimeter. In the implementation, time step of 1 s is considered to measure the traffic states ( $x_{t+1}$ ) of the system whereas the optimal control actions ( $u_0^*(t)$ ) and references  $\beta_i^r(t)$  are updated at each 60 s. In this work, we used the MATLAB environment to synthesize simulations and LP and NLP are solved using the Interior Point Method (IPM) method. Prediction horizon ( $N$ ), output penalty ( $Q$ ), and input penalty ( $R$ ) were set to 10,  $0.001 \times \mathbb{I}_{(n_y \times n_y)}$ , and  $100 \times \mathbb{I}_{(n_u \times n_u)}$ , respectively. The constraints on the input flow rate were set to  $0.1 \leq u_k \leq 6$  veh/s. The values of constraints are determined based on the uncontrolled simulations.

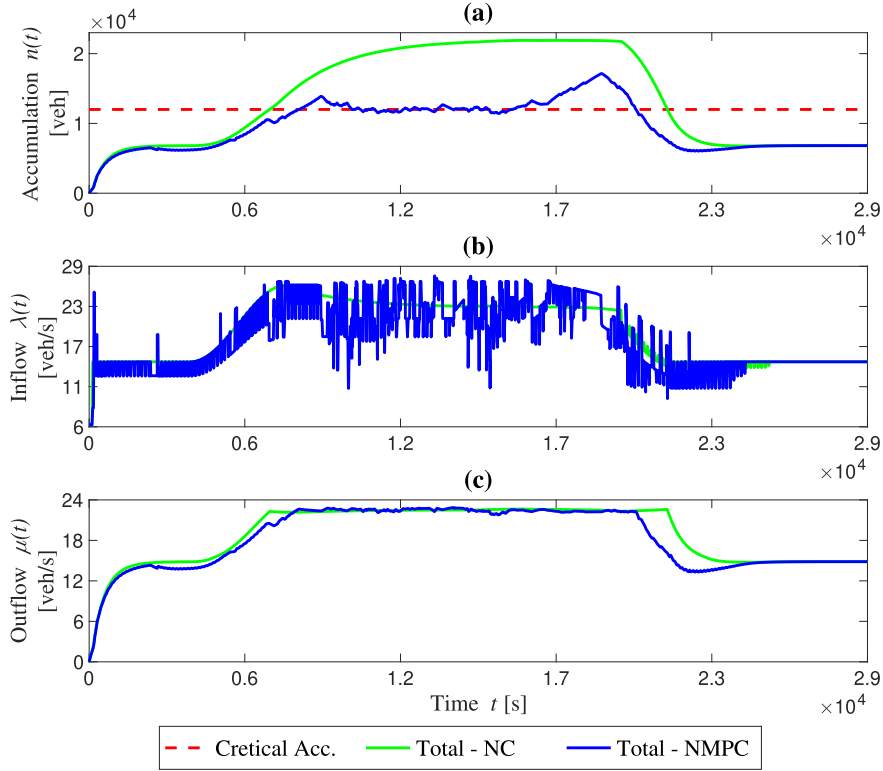


Fig. 8. Response of total accumulation (a), inflow (b), and outflow (c) inside the reservoir for nocontrol and network-wide NMPC.

## 6. Simulation results

To demonstrate the effectiveness of the designed NMPC and optimal routing strategy, a case study is considered and the results are compared with the Nocontrol (NC) case. The values of the MFD model parameters used in the case study are given in Table 1.

To create the congestion scenario, the inflow demand for the internal trip was kept high for a total simulation time of 8 h. Fig. 4 shows the inflow demand profiles of routes ( $R_1, \dots, R_7$ ) used in the case study.

### 6.1. Network-wide emission control

Fig. 5 shows the response of NMPC strategy while tracking  $\beta_i^r(t)$  values. For control case, during the network loading period measured  $\beta_i(t)$  values are zero as shown in the zoom part of Fig. 5(a), during that time there was no outflow at the exit of the reservoir. After that, there was a gradual increase in the outflows and a decrease in the  $\beta_i(t)$  values. The spike in the  $\beta_i(t)$  was due to the first outputs at the exit of the reservoir. However, it can be observed that in some parts especially during high inflow demands (from 3600–21000 s),  $\beta_2$  and  $\beta_4$  values are trying to catch references but this is not possible due to the DUE discipline which enforces the limitation on the number of users.

On the other hand,  $\beta_5$  and  $\beta_6$  are able to track references for a long duration. In cases of  $\beta_3$  and  $\beta_7$  reference values oscillate during high demand and accumulation and NMPC is trying to optimally track these reference values considering the DUE. For  $\beta_3$  and  $\beta_7$ , reference values oscillate between 0 and 1, which is because of routes  $R_3$  and  $R_7$  have the longest trip lengths. For the NC case,  $\beta_2, \beta_3, \beta_5, \beta_6$  and  $\beta_7$  values oscillate during high congestion, except for  $\beta_4$  which is due to the highest outflow on the  $R_4$ .

Fig. 6 depicts the emission levels of  $\text{NO}_x$  and  $\text{CO}_2$  and mean speed in the whole network (left column) and the reservoir (right column). Note here that  $\text{CO}_2$  is only monitored and is not taken into account in the calculation of  $\beta_i(t)$ . It can be observed that, with the proposed strategy there is a significant decrease in the network-wide and reservoir emissions and an increase in mean speeds. With NMPC, the amount of  $\text{NO}_x$  is reduced by 235 kg and  $\text{CO}_2$  by 15854 kg. It indicates that the proposed strategy is beneficial for the perimeter area as well as in total.

Fig. 7 depicts the total emission levels of  $\text{NO}_x$  and  $\text{CO}_2$  and mean speed on the inbound link (left column) and the bypass (right column). With NMPC, on the inbound links total (sum of  $IL_i$ ) emissions are reduced and mean speed is increased. This result may look contradictory because the main point of our strategy is to introduce queues on inbound links to detour vehicles to bypass routes. A closer look at the results shows that the control acts more smartly. During the onset of congestion, it first restricts sooner the inflow at route 7 and diverting flow on the bypass route. Besides that, it increases the outflow from the reservoir improving traffic conditions with higher speed. So, queues are in the end in total less severe in inbound links than for the uncontrol case due to the combination of

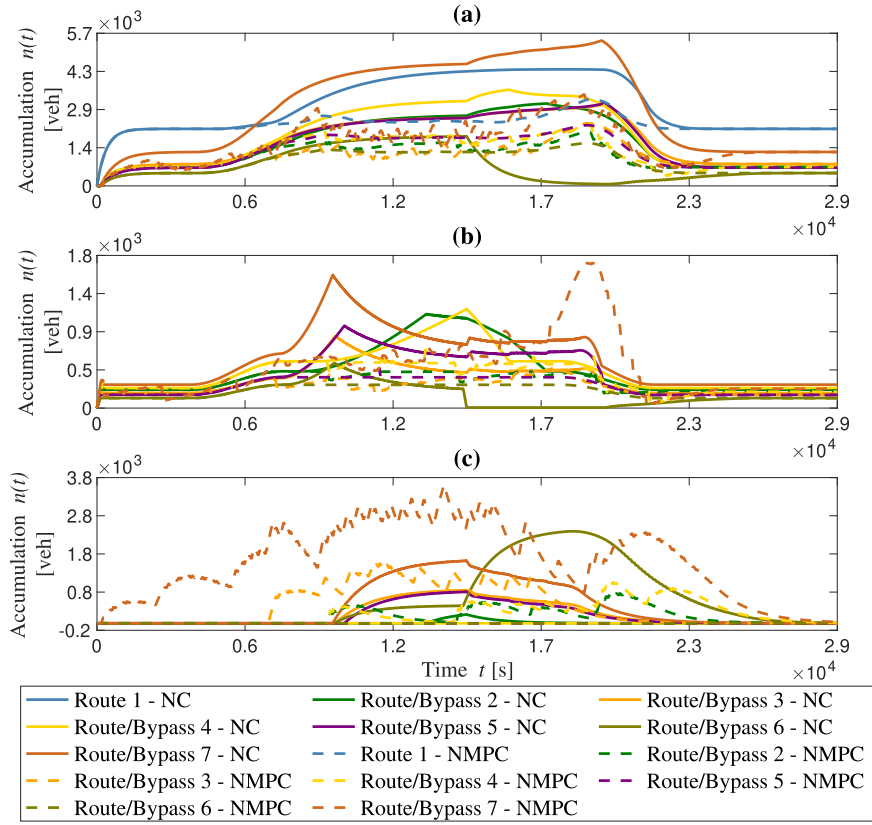


Fig. 9. Response of accumulation in the reservoir (a), inbound links (b), and bypass (c) for nocontrol and network-wide NMPC.

these two effects. Between time 1570–1970 s, emissions on the bypass is reduced below the NC due to the decrease in the accumulation on the bypass (see Fig. 9)) and increase in the accumulation of reservoir (see Fig. 8(a)). The oscillations in the mean speed are due to the inflow which is also oscillating (see Fig. 8(e)). As expected, with NMPC bypass have high emissions as compared to the NC. This is due to the fixed mean speed on all the bypasses.

Fig. 8 presents the total accumulation, inflow, and outflow inside the reservoir. It can be seen that during the loading and unloading period the total accumulation inside the perimeter is almost similar in NC and NMPC cases. During the high demand period, the NC drives the reservoir in high congestion sooner as compared to the NMPC case and the opposite effect can be seen during the unloading period. Moreover, total accumulation with the NMPC case is around the critical value which keeps good traffic conditions in the reservoir. The bump in the accumulation (from 1700 to 2000 s) is due to the more inflow to track  $\beta_i^r(t)$  which has reduced the mean speed inside the reservoir.

Fig. 9 shows the accumulation on each route inside the reservoir (a), inbound link/queue (b) and accumulation on the bypass (c). For the nocontrol case, all routes inside the reservoir have high congestion except on route 6 and for network-wide control case accumulations are significantly reduced. It can be seen that for the nocontrol case during high demand period except IL 6 all other IL has long queues and with NMPC queues are reduced due to the increased mean speeds and increased inflow to the reservoir. In the case of the bypass routes,  $F_7$  and  $F_3$  have more accumulation with NMPC case due to the trip length of  $R_7$  and  $R_3$ .

Fig. 10 (a) shows the route-wise TTS and (b) total (sum of reservoir, ILs, and bypass) in the network, and exit production of the network in Fig. 10 (c). It can be observed that the total TTS with NMPC is less which is better for the users to finish their trips in less time. The exit production is calculated as the sum of all route outflows multiplied by their trip length inside the reservoir:

$$P_{\text{out}}(t) = \sum_{i=1}^R L_i q_{\text{out},i}(t). \quad (23)$$

$P_{\text{out}}(t)$  shows the performance of the network under free-flow and congestion states. For the NC case, we observe over-saturation in the reservoir as the accumulation  $n(t)$  exceeds the critical accumulation  $n_c$ .

#### 6.1.1. Performances with different demand profiles

To further test the performance of the proposed network-wide NMPC under higher and lower congestion levels, we run again the simulation with scale-up and down demand profiles i.e., baseline (shown in Fig. 4) remains the same but the total number of generated vehicles is first increased by 5 and 10% and then decrease by 5, 10, 15, and 20%. Note that the reference demand profile

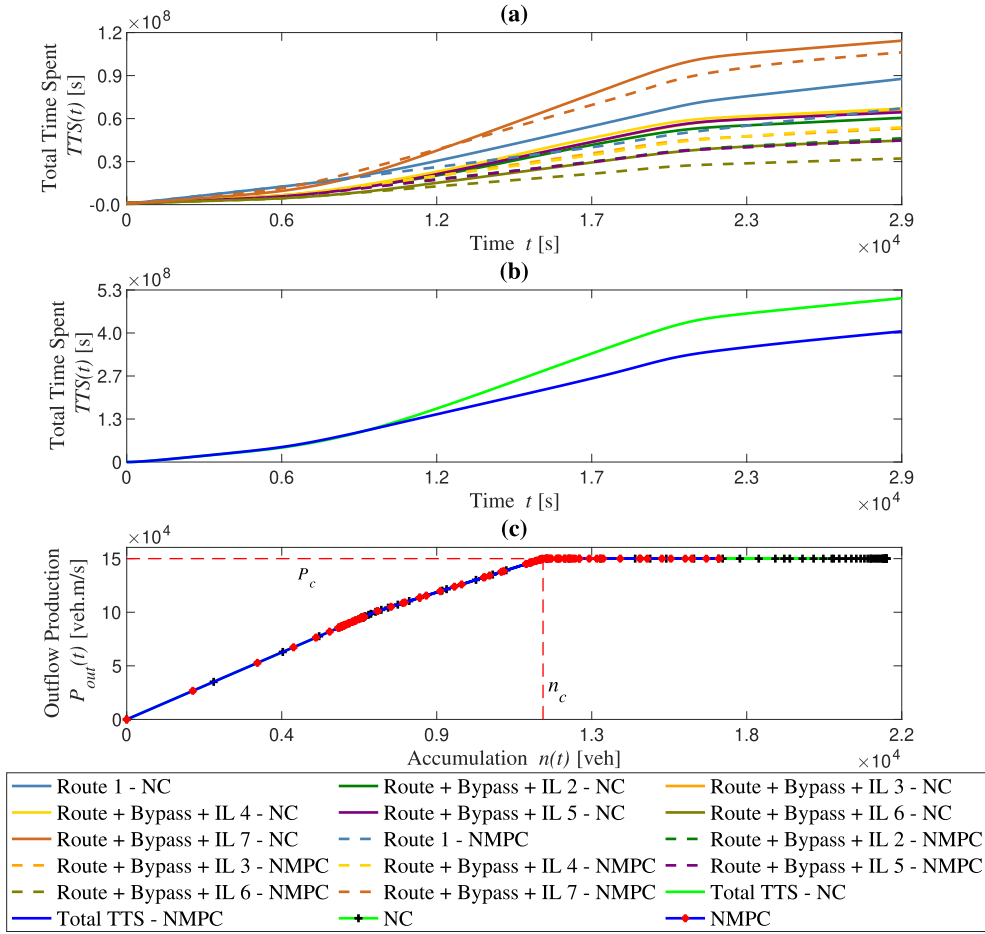


Fig. 10. Response of route-wise TTS (a), total TTS (b), and production MFD (c) at the exit for nocontrol and network-wide NMPC.

shown in Fig. 4 is already designed to have enough congestion inside the network for the nocontrol case. This will show the performance of the network-wide NMPC and give us operating conditions when it performs better as compared to the nocontrol case.

Fig. 11 shows the performance improvement ( $\text{NO}_x$  emission reduction) of the proposed network-wide emission control strategy when compared with the nocontrol case. Original demand profile (0% in Fig. 11) shows the  $\text{NO}_x$  emission reduction of 9.34% as compared to nocontrol case. When we increase the demands by 5%, congestion inside the reservoir increases above critical but still it is less than in nocontrol case. Due to the DUE, accumulation on inbound links and bypass increases which consequently increases the emissions. It is observed that during loading and unloading period emissions on bypass increases (as compared to nocontrol case) which is then compensated by decrease in emissions on IL and inside the reservoir. Overall, the emissions obtained by network-wide controller are better than nocontrol case but the reduction is moderate. Next, we increased the demands by 10% which creates very high congestion inside the reservoir. DUE moves vehicles to IL and bypass which generates high emissions. Similar to the 5% situation, during loading and unloading periods emission increases on bypass but increase is much higher and it is slightly compensated during congestion period on IL and inside the reservoir. In this situation of demands, network-wide controller shows only minor improvement in  $\text{NO}_x$  emission as compared to the nocontrol case. We further tested the performance with increasing demands by 20% but the demands are so high that network-wide NMPC shows no improvement and increase the emissions as compared to the nocontrol case. However, it should be noted that, this scenario is relatively very congested. With this more demand, the inner-city goes to the gridlock.

We performed the tests with scaling down the demands by 5% which shows the high congestion in the nocontrol case and minor congestion in the control case. Here we observed that during the congestion period NMPC performs very well and tracks desired references which are around 0.5 for  $\beta_3$  and  $\beta_7$  and other  $\beta$  are around 0. Due to the DUE and well tracking of optimal coefficients by NMPC, there is a significant reduction of emissions inside the reservoir and IL, but at the same time increase on bypass. As there is less demand, during the congestion period, the mean speed inside the reservoir and IL increased and reservoir accumulation is above and around  $n_c$ .

Similarly, we scaled down demands by 10% which shows high congestion in nocontrol and minor congestion in the control case. The same response is observed as that of -5% but in this case accumulation inside the reservoir is below and around  $n_c$  which helps

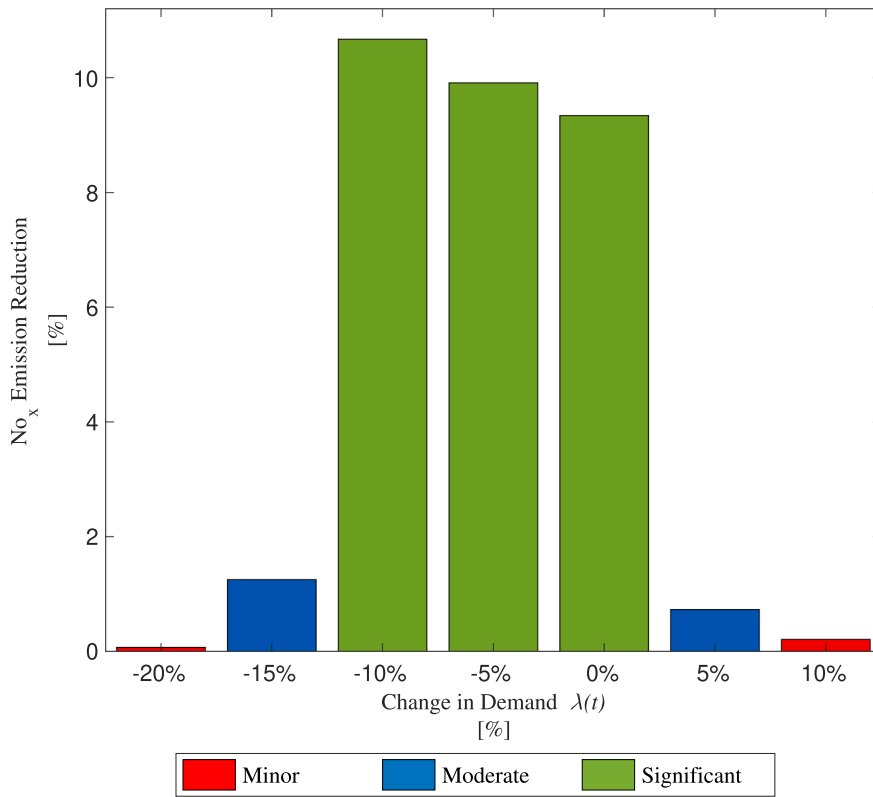


**Fig. 11.** Performance of the proposed network-wide NMPC strategy with different demand profiles. The percentage on the x-axis indicates the percentage increase or decrease in demand profile relative to the baseline (as shown in Fig. 4) demand and y-axis indicate the NO<sub>x</sub> emission reduction by network-wide NMPC as compared to the nocontrol case.

to reduce emissions in the reservoir and IL. As a result of that, we get a significant reduction in the whole network. We further decreased the demands by 15%, which shows minor congestion in the both control and uncontrol cases. In this case, only  $\beta_7$  reference is around 0.5 and the other  $\beta$  are references are 0. DUE and NMPC divert fewer vehicles to bypass and IL as there is less demand. The emissions on the bypass are increased, which is compensated by emissions in the reservoir and IL. Overall, the emission reduction is 1.25% as compared to the nocontrol case.

We again decreased the demands by 20%, which shows no congestion in control and nocontrol case. In this case,  $\beta_3$  and  $\beta_7$  references are 1 and other 0. But, NMPC is can not track the desired reference due to the less demand and there is no accumulation on bypass and IL. The mean speed in the reservoir and IL is almost the same in the nocontrol and control case. Overall, there is a minor reduction in the emissions due to the reduction in emissions in the reservoir. For further scaled down demand by  $-30\%$ , there is no reduction in emissions as compared to no control case.

The above results show that the proposed network-wide emission control strategy shows improvements for the demands which generates minor to moderate congestion inside the reservoir. For these demands (0%,  $-5\%$ , and  $-10\%$ ) it is observed that the accumulation inside the reservoir is around  $n_c$  which means the proposed strategy not only reduces emissions but also maintains the congestion in the reservoir around  $n_c$ .

## 6.2. Comparison with other control strategies

This section discusses the performance comparison of four control strategies designed for different objectives: (I) classical perimeter control strategy designed for traffic congestion control inside the reservoir, (II) reservoir emission control strategy designed for NO<sub>x</sub> emission control only inside the reservoir, (III) our proposed strategy designed for network-wide emission control, which we presented in Sections 4 and 5, and (IV) network-wide congestion control.

### 6.2.1. Strategy I: classical perimeter (reservoir congestion) control

In the last few years, perimeter control strategies were focused on increasing the throughput of a given region with few concerns about the impacts on emission inside and more important outside the controlled area. Authors in Zegeye et al. (2009) showed that this is not marginal. To compare the performance of the proposed approach, a classical perimeter control strategy is designed to improve traffic conditions inside the reservoir by maximizing the throughput. Here we used the NMPC strategy to track the total accumulation ( $n$ ) in the reservoir to critical accumulation ( $n_c$ ) value which was set to 12000 veh. In the NMPC, CFTOC problem



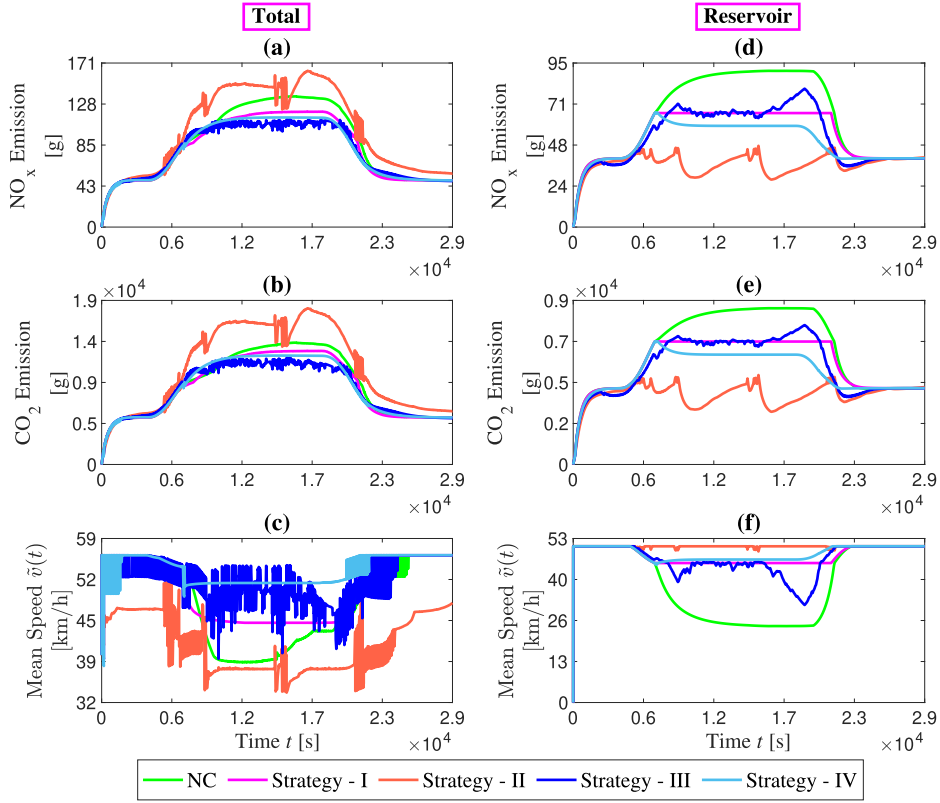


Fig. 12. Response of total (left column) and reservoir (right column) emissions and mean speed for nocontrol case and four control strategies.

similar to (22) was used with objective function as follows:

$$\min_{u_0, \dots, u_{N-1}} \sum_{k=0}^{N-1} (\|n_k - n_{c,k}\|_Q^2 + \|\Delta u_k\|_R^2), \quad (24a)$$

$$\text{s. t. } (22b) - (22g), \quad (24b)$$

where  $n_c$  corresponds to the reference value of total accumulation and  $n$  corresponds to the predicted total accumulation. The used NMPC settings were the same as in Section 5.3 except the control update time which is 1 s. Here, simulation time step is 1 s.

### 6.2.2. Strategy II: reservoir emission control

The instantaneous emission curves for  $\text{NO}_x$  and  $\text{CO}_2$  are given in Fig. 3. As the free-flow speed inside the reservoir is 50.4 km/h, all the possible emission levels are represented by the decreasing left branches of both curves. Thus, to minimize the instantaneous emission inside the reservoir, we need to keep the speed levels close to the free-flow speed since travel distances are constant inside the reservoir. The emissions can be minimized inside the reservoir if they are equal to zero, but this will force all the vehicles to take a longer alternative and significantly generate higher total emissions in the network. To reduce the emission inside the reservoir, we designed a NMPC strategy to track optimal mean speed ( $\tilde{v}^r = 50$  km/h) which corresponds to low-emission levels.

In the NMPC, CFTOC problem similar to (22) was used with the objective function as follows:

$$\min_{u_0, \dots, u_{N-1}} \sum_{k=0}^{N-1} (\|\tilde{v}_k - \tilde{v}_k^r\|_Q^2 + \|\Delta u_k\|_R^2), \quad (25a)$$

$$\text{s. t. } (22b) - (22g), \quad (25b)$$

where  $\tilde{v}^r$  corresponds to the reference value of free-flow speed inside the reservoir and  $\tilde{v}$  corresponds to the predicted mean speed in the reservoir. Here, control update time is set to 60 s and simulation time step is 1 s.

### 6.2.3. Strategy IV: network-wide congestion control

Our two-layer control framework can be easily extended to account for other objective function at the network-level. For example here, we change the emission minimization in (19) by a total travel time minimization and compare the overall performance. Similar to the network-wide emission control problem, we solve the LP problem to estimate optimal  $\beta_i^r(t)$  that minimizes the total

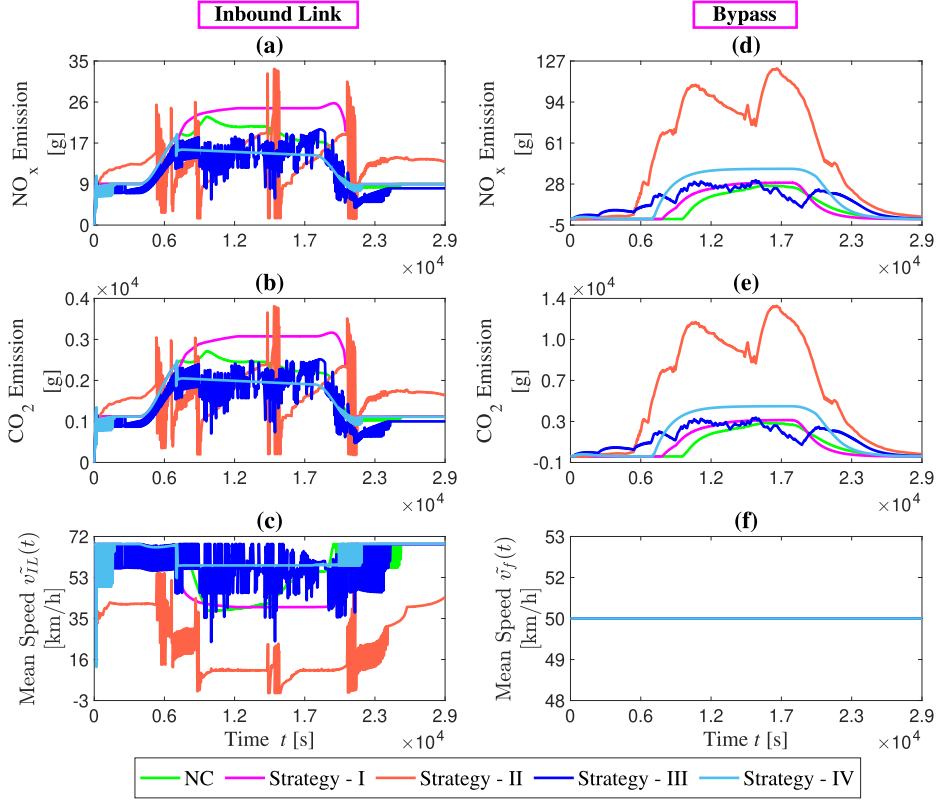


Fig. 13. Response of inbound link (left column) and bypass (right column) emissions and mean speed for nocontrol case and four control strategies.

accumulation ( $A_\tau$ ) for a predefined time horizon of  $\tau = 60$  s. The network-wide accumulation at each  $\tau$  is calculated by assuming the fixed accumulation and speed (equal to the values at  $t$ ) for  $[t, t + \tau]$ . The predicted  $A_\tau$  for each simulation time step between  $[t, t + \tau]$  is calculated as follows:

$$A_{\tau,F}(t) = \frac{\lambda_i(t) \times \tau \times L_{F,i}}{\tilde{v}_F(t)}, \quad (26a)$$

$$A_{\tau,res.}(t) = \frac{\lambda_i(t) \times \tau \times L_i}{v(t)}, \quad (26b)$$

$$A_{\tau,IL}(t) = \frac{\lambda_i(t) \times \tau \times L_{IL,i}}{v_{IL,i}(t)}. \quad (26c)$$

Combining (26a)-(26c) and considering the optimal splitting coefficient, we get total accumulation in the network as:

$$A_\tau(t) = A_{\tau,F}(t)\beta_i^r(t) + (A_{\tau,res.}(t) + A_{\tau,IL}(t))(1 - \beta_i^r(t)). \quad (27a)$$

To find the optimal splitting coefficient  $\beta_i^r(t)$  at each time step  $t$  an LP problem is formulated as:

$$\min_{\beta_i^r(t)} A_{\tau,F}(t)\beta_i^r(t) + (A_{\tau,res.}(t) + A_{\tau,IL}(t))(1 - \beta_i^r(t)), \quad (28a)$$

$$\text{s. t. } 0 \leq \beta_i^r(t) \leq 1, \quad \forall t \in [t, t + \tau]. \quad (28b)$$

After obtaining the  $\beta_i^r(t)$  values for all time step between  $[t, t + \tau]$ , we apply a simple filtering technique corresponding to the moving average as given in (20). The obtained  $\beta_i^r(t)$  values are considered as the reference for the network-wide accumulation control strategy in layer 2 for each time step  $t$  over the time horizon  $[t, t + \tau]$ . The values of controlled variable  $\beta_i(t)$  in the simulator were estimated at the exit of the reservoir based on the outflow observation as given in (21).

#### 6.2.4. Performance comparison

Fig. 12 shows the evaluation of total (network-wide) and reservoir emissions for all four control strategies. It can be seen for total  $\text{NO}_x$  and  $\text{CO}_2$  emissions that during the network loading period (1–6000 s), all strategies show similar response as nocontrol case. However, for the network-wide case during the high demand period, strategy II shows the highest emissions due to the reduced mean

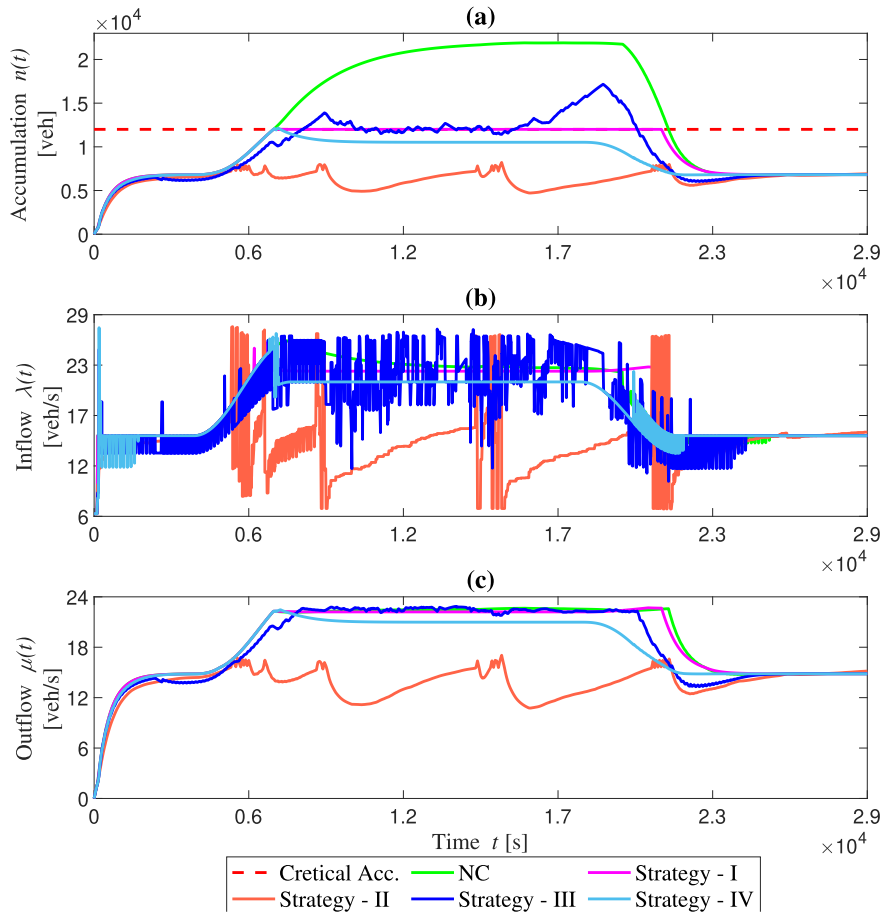


Fig. 14. Response of accumulation (a), inflow (b), and outflow (c) inside the reservoir for nocontrol case and four control strategies.

speed, as the designed controller is better for reservoir and not for the whole network and strategy III shows the lowest emissions due to the increased speed as NMPC is designed to reduce network-wide emissions. This shows the effectiveness of the network-wide emission control strategy. Strategies I and IV show emission values between strategies II and III which is as expected due to the objective functions of the NMPC.

In the reservoir, during the loading period, strategy II shows the lowest emissions due to the highest possible mean speed. For the high demand period, all four control strategies show reduced emission levels as compared to the nocontrol case due to the increased mean speed in the reservoir. As expected, strategy II shows the lowest emissions among all strategies as controller tracks desired mean speed which gives the lowest emissions. Strategy IV shows less emissions as compared to strategies II and III. This is due to the reduced accumulation (see Fig. 14) and increased mean speed in the reservoir. Emissions of strategy III in the reservoir are higher than for control strategies but at the same time the accumulation is around  $n_c$  which utilizes the optimal capacity of the reservoir.

Fig. 13 shows the emissions and speed in the inbound link and bypass routes for all four strategies. On the inbound links strategy I shows the highest emissions whereas strategy III shows the lowest. The mean speed in strategy II is reduced and shows up and down peaks which gives more emissions at those peaks but on average, the emission level of strategy II is lower than strategy I. Strategy IV shows better emissions than strategies I and II but a little bit higher than III, this is due to the lower accumulation (see Fig. 15 (a)) and higher mean speed in strategy IV.

On the bypass routes, strategy II gives the highest emission levels due to the increased accumulation as bypass speed is constant. Also, strategy I shows less emissions than other strategies due to reduced accumulation. The nocontrol case shows the lowest emissions due to the low accumulation on the bypass. However, it shows the highest emission and accumulation in the reservoir. The higher emissions for strategy IV as compared to I and III is due to the higher accumulation.

Fig. 14 shows the comparison of accumulation, inflow, and outflow inside the reservoir for all four control strategies. As expected, strategy I keeps accumulation at  $n_c$ . Strategy II shows the lowest accumulation as it is designed to track the mean speed in the reservoir, which keeps low inflow and outflow. Strategy III shows accumulation around  $n_c$  due to the DUE and gating controller which tries to keep network-wide emissions at the desired green routing coefficients. Strategy IV shows accumulation lower than  $n_c$  as DUE and gating controller detour more vehicles to the bypass routes due to the higher mean speed and high capacity of the bypass routes. Also, strategy IV shows lower inflow and outflow than strategies I and III.

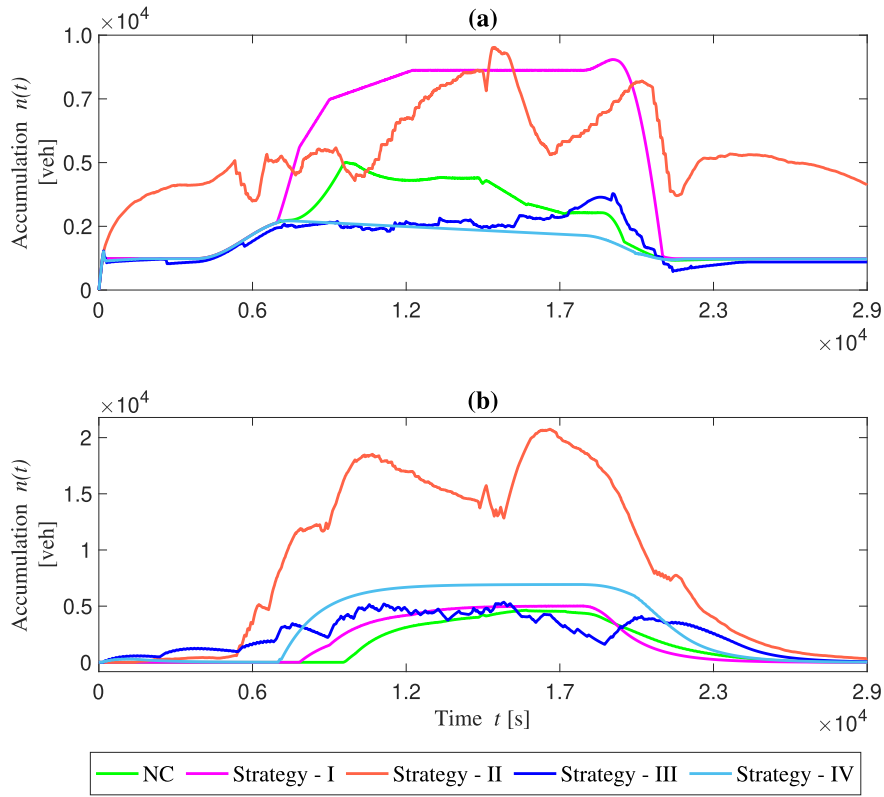


Fig. 15. Response of inbound link accumulation (a) and bypass accumulation (b) for nocontrol case and four control strategies.

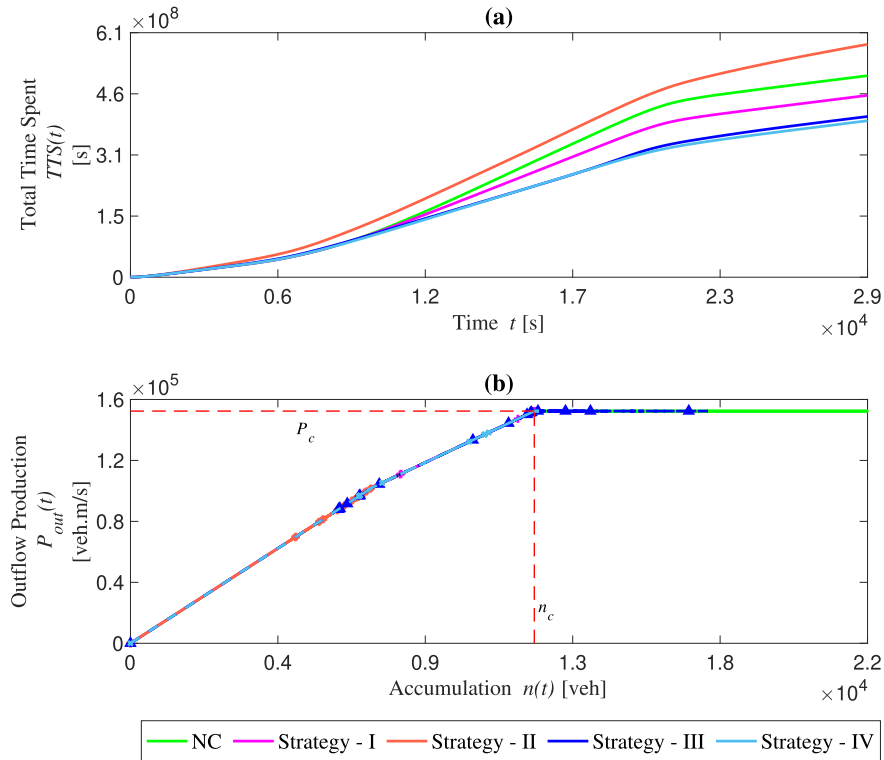


Fig. 16. Response of TTS (a) and production MFD (b) at the exit for nocontrol case and four control strategies.

**Table 2**  
Performance comparison of uncontrol and gating control approaches for different objectives.

Case	Indicator	Reservoir	IL	Bypass	Total
I	Emission NO <sub>x</sub>	-16.15	18.51	18.65	-6.92
	Emission CO <sub>2</sub>	-11.92	19.47	18.65	-3.28
	TTS	-25.30	2.76	-29.06	-9.02
	Mean Speed	22.94	-5.86	0	3.67
II	Emission NO <sub>x</sub>	-43.13	-5.22	464.1	15.36
	Emission CO <sub>2</sub>	-39.11	-6.44	464.1	21.09
	TTS	-30.09	28.99	0.01	13.67
	Mean Speed	30.62	-58.62	0	-15.21
III	Emission NO <sub>x</sub>	-17.52	-18.16	62.81	-9.34
	Emission CO <sub>2</sub>	-6.01	-14.17	62.81	-6.01
	TTS	-19.65	-23.37	-24.11	-19.65
	Mean Speed	20.08	4.75	0	7.13
IV	Emission NO <sub>x</sub>	-23.52	-14.96	109.46	-7.61
	Emission CO <sub>2</sub>	-19.23	-11.81	109.46	-3.46
	TTS	-26.40	-29.61	-30.08	-21.22
	Mean Speed	24.98	8.64	0	9.96

Fig. 15 shows the accumulation on the inbound link and bypass route. On the inbound link, strategy IV shows the lowest accumulations due to the increased mean speed whereas strategy II shows the highest accumulation due to the decreased speed.

For bypass routes, strategy II shows the highest accumulation as it tries to keep a higher mean speed in the reservoir by decreasing inflow to the reservoir through the gating controller. So, more vehicles detour to the bypass or creates queue at the inbound link.

Fig. 16 shows the TTS and exit production MFD for four strategies used to track different objectives. Due to the increased accumulation on the inbound link and bypass, strategy II shows the highest TTS whereas strategy IV shows the lowest TTS due to the less accumulation on IL and the reservoir. The low TTS for strategy IV is expected as this one is supposed to give the best traffic conditions, i.e., the lowest delays and thus lowest TTS.

Fig. 16(b) illustrates the evolution of  $P_{out}(t)$  versus  $n(t)$  for four strategies. For the nocontrol case, we can observe over-saturation at 150000 veh/m/s in the reservoir as the accumulation  $n(t)$  exceeds the critical accumulation  $n_c$ . For strategy II production is around 111000 veh/m/s at 8200 veh and strategy III has an exit production of 150000 veh/m/s at accumulation 17000 veh which is a little higher than critical accumulation. Due to accumulation tracking in strategy I, its accumulation is at  $n_c = 12000veh$  and exit production at 150000 veh/m/s. For strategy IV, accumulation in the reservoir is 12145veh and exit production is 150000 veh/m/s. Table 2 gives the summary of Key Performance Indicators (KPIs) used to compare uncontrol and four control strategies. Given values in the table are calculated for the whole simulation time (28800 s/8 h) in the form of percentage (%) with respect to the uncontrolled case. Values indicated in red show a negative effect and values in green show a significant positive effect of the control case, whereas values in black indicate no effect.

## 7. Conclusions

This paper proposed an efficient network-wide emission control strategy, that balances traffic conditions in the inner-city and the suburb network to minimize total emission in the full network. We developed a new methodological modeling framework, that predicts traffic dynamics and the consequences of the control actions. It combines an accumulation-based MFD model for the inner-city and simple conservation laws for inbound links and the suburb network. Users follow a classical UE discipline when arbitrating between several routing alternatives.

The control strategy is composed of two layers. The first layer is the optimal green routing and determine the splitting coefficients ( $\beta_i^r(t)$ ) which give the optimal route choice corresponding to low emission route between inner-city and suburb routes. The values of the splitting coefficients from the first layer are then utilized as the reference for perimeter control in the second layer. While this first layer resorts to very simple assumptions about traffic dynamics, i.e., traffic states are supposed stationary over the optimization horizon, the simulation results prove that, this is sufficient to provide accurate enough  $\beta_i^r(t)$  values as references for the gating strategy. This is very interesting as this shows that we can resort to a very rough but fast optimization framework at this level to monitor the optimal distribution of OD flow over the different alternatives at the city level. Here the simulations highlight that what really matters is to start the diversion of vehicles to suburb routes at the right time, i.e., when congestion is not yet established rather than following a very rigorous splitting scheme. The second layer is the NMPC-based gating control strategy. NMPC is developed based on our modeling framework to track green emission coefficients (obtained from layer 1) by regulating the optimal entry flows to the city center. The proposed approach is demonstrated through traffic simulation by considering a case study involving six OD pairs and six bypass routes.

Presented results showed that the proposed control strategy can reduce network-wide NO<sub>x</sub> emission by 9.34% and CO<sub>2</sub> emission by 6.01% along with the decrease in the TTS by 19.65% as compared to nocontrol strategy. Moreover, the proposed strategy also helps to protect the reservoir from severe congestion. The performance of the developed approach is demonstrated and compared with three other control strategies designed for (i) classical perimeter control for traffic congestion control inside the reservoir (ii) emission control inside the reservoir, and (iii) network-wide congestion control. Comparative analysis shows that the proposed strategy outperforms other strategies. To broaden the validity of the results, in the future we are aiming to consider a multi-reservoir city network and look for on-field experimentation.

## Acknowledgments

The research leading to these results has received funding from the European Research Council (ERC) under the European Union's Horizon 2020 research and innovation program (grant agreement No 646592 – MAGNUM project).

## References

- Basark, L.D., De Schutter, B., Hellendoorn, H., 2012. Traffic management for automated highway systems using model-based predictive control. *IEEE Trans. Intell. Transp. Syst.* 13 (2), 838–847.
- Borrelli, F., Bemporad, A., Morari, M., 2017. Predictive control for linear and hybrid systems. Cambridge University Press.
- CARB, 2017. EMFAC 2017 User's Guide.
- Cavallaro, F., Giaretta, F., Nocera, S., 2018. The potential of road pricing schemes to reduce carbon emissions. *Transp. Policy* 67, 85–92.
- Chen, J., Yu, Y., Guo, Q., 2019. Freeway traffic congestion reduction and environment regulation via model predictive control. *Algorithms* 12 (10), 220.
- Chen, L., Yang, H., 2012. Managing congestion and emissions in road networks with tolls and rebates. *Transport. Res. Part B: Methodol.* 46 (8), 933–948.
- Choudhary, A., Gokhale, S., 2016. Urban real-world driving traffic emissions during interruption and congestion. *Transport. Res. Part D: Transp. Environ.* 43, 59–70.
- Csikós, A., Tettamanti, T., Varga, I., 2015. Macroscopic modeling and control of emission in urban road traffic networks. *Transport* 30 (2), 152–161.
- Csikós, A.A., Varga, I., Hangos, K., 2018. A hybrid model predictive control for traffic flow stabilization and pollution reduction of freeways. *Transport. Res. Part D: Transp. Environ.* 59, 174–191.
- Daganzo, C.F., 2007. Urban gridlock: Macroscopic modeling and mitigation approaches. *Transport. Res. Part B: Methodol.* 41 (1), 49–62.
- Ding, H., Guo, F., Zheng, X., Zhang, W., 2017. Traffic guidance–perimeter control coupled method for the congestion in a macro network. *Transport. Res. Part C: Emerg. Technol.* 81, 300–316.
- EPA, U., 2003. User's guide to MOBILE 6.1 and MOBILE 6.2 Mobile Source Emission Factor Model.
- EPA, U., 2014. Motor vehicle emission simulator (MOVES), user guide for MOVES2014.
- Ferrara, A., Saccone, S., Siri, S., 2018. Freeway Traffic Modelling and Control. Springer.
- Franco, V., Kousoulidou, M., Muntean, M., Ntziachristos, L., Hausberger, S., Dilara, P., 2013. Road vehicle emission factors development: a review. *Atmos. Environ.* 70, 84–97.
- Frejo, J.R.D., Núñez, A., De Schutter, B., Camacho, E.F., 2014. Hybrid model predictive control for freeway traffic using discrete speed limit signals. *Transport. Res. Part C: Emerg. Technol.* 46, 309–325.
- Fu, H., Liu, N., Hu, G., 2017. Hierarchical perimeter control with guaranteed stability for dynamically coupled heterogeneous urban traffic. *Transport. Res. Part C: Emerg. Technol.* 83, 18–38.
- Fujita, E.M., Campbell, D.E., Zielinska, B., Chow, J.C., Lindhjem, C.E., DenBleyker, A., Bishop, G.A., Schuchmann, B.G., Stedman, D.H., Lawson, D.R., 2012. Comparison of the MOVES 2010a, MOBILE 6. 2, and EMFAC 2007 mobile source emission models with on-road traffic tunnel and remote sensing measurements. *J. Air Waste Manage. Assoc.* 62 (10), 1134–1149.
- Geroliminis, N., 2015. Cruising-for-parking in congested cities with an MFD representation. *Econ. Transport.* 4 (3), 156–165.
- Geroliminis, N., Daganzo, C.F., 2008. Existence of urban-scale macroscopic fundamental diagrams: Some experimental findings. *Transport. Res. Part B: Methodol.* 42 (9), 759–770.
- Geroliminis, N., Haddad, J., Ramezani, M., 2013. Optimal perimeter control for two urban regions with macroscopic fundamental diagrams: A model predictive approach. *IEEE Trans. Intell. Transp. Syst.* 14 (1), 348–359.
- Godfrey, J., 1969. The mechanism of a road network. *Traffic Eng. Control* 8 (8).
- Groot, N., De Schutter, B., Hellendoorn, H., 2013. Integrated model predictive traffic and emission control using a piecewise-affine approach. *IEEE Trans. Intell. Transp. Syst.* 14 (2), 587–598.
- Grüne, L., Pannek, J., 2017. Nonlinear Model Predictive Control: Theory and Algorithms. Communications and Control Engineering, second ed. Springer, Cham,

- Switzerland.
- Haddad, J., Ramezani, M., Geroliminis, N., 2013. Cooperative traffic control of a mixed network with two urban regions and a freeway. *Transport. Res. Part B: Methodol.* 54, 17–36.
- Haddad, J., Shraiber, A., 2014. Robust perimeter control design for an urban region. *Transport. Res. Part B: Methodol.* 68, 315–332.
- Hajiahmadi, M., Haddad, J., De Schutter, B., Geroliminis, N., 2015. Optimal hybrid perimeter and switching plans control for urban traffic networks. *IEEE Trans. Control Syst. Technol.* 23 (2), 464–478.
- Han, Y., Hegyi, A., Yuan, Y., Roncoli, C., Hoogendoorn, S., 2018. An extended linear quadratic model predictive control approach for multi-destination urban traffic networks. *IEEE Trans. Intell. Transp. Syst.* 20 (10), 3647–3660.
- Han, Y., Ramezani, M., Hegyi, A., Yuan, Y., Hoogendoorn, S., 2020. Hierarchical ramp metering in freeways: an aggregated modeling and control approach. *Transport. Res. Part C: Emerg. Technol.* 110, 1–19.
- Ingole, D., Mariotte, G., Leclercq, L., 2019. Nonlinear model predictive control to reduce network-wide traffic emission. *IFAC-PapersOnLine* 52 (6), 19–24.
- Ingole, D., Mariotte, G., Leclercq, L., 2020. Perimeter gating control and citywide dynamic user equilibrium: a macroscopic modeling framework. *Transport. Res. Part C: Emerg. Technol.* 111, 22–49.
- Jamshidnejad, A., Papamichail, I., Papageorgiou, M., De Schutter, B., 2017. Sustainable model-predictive control in urban traffic networks: Efficient solution based on general smoothing methods. *IEEE Trans. Control Syst. Technol.* 26 (3), 813–827.
- Keller, M., 2017. *Handbook of emission factors for road transport (HBEFA)* 3.3.
- Kim, S., Tak, S., Lee, D., Yeo, H., 2019. Distributed model predictive approach for large-scale road network perimeter control. *Transp. Res. Rec.* 2673 (5), 515–527.
- Kouvelas, A., Saeedmanesh, M., Geroliminis, N., 2017a. Enhancing model-based feedback perimeter control with data-driven online adaptive optimization. *Transport. Res. Part B: Methodol.* 96, 26–45.
- Kouvelas, A., Saeedmanesh, M., Geroliminis, N., 2017b. A linear formulation for model predictive perimeter traffic control in cities. *IFAC-PapersOnLine* 50 (1), 8543–8548.
- Lejri, D., Can, A., Schiper, N., Leclercq, L., 2018. Accounting for traffic speed dynamics when calculating copert and phem pollutant emissions at the urban scale. *Transport. Res. Part D: Transp. Environ.* 63, 588–603.
- Li, Z., Jin, S., Xu, C., Li, J., 2019. Model-free adaptive predictive control for an urban road traffic network via perimeter control. *IEEE Access* 7, 172489–172495.
- Lin, S., De Schutter, B., Xi, Y., Hellendoorn, H., 2013. Integrated urban traffic control for the reduction of travel delays and emissions. *IEEE Trans. Intell. Transp. Syst.* 14 (4), 1609–1619.
- Liu, W., Geroliminis, N., 2017. Doubly dynamics for multi-modal networks with park-and-ride and adaptive pricing. *Transport. Res. Part B: Methodol.* 102, 162–179.
- Long, J., Szeto, W., 2019. Congestion and environmental toll schemes for the morning commute with heterogeneous users and parallel routes. *Transport. Res. Part B: Methodol.* 129, 305–333.
- Luo, L., Ge, Y.-E., Zhang, F., Ban, X.J., 2016. Real-time route diversion control in a model predictive control framework with multiple objectives: Traffic efficiency, emission reduction and fuel economy. *Transport. Res. Part D: Transp. Environ.* 48, 332–356.
- Mahmassani, H.S., Williams, J.C., Herman, R., 1984. Investigation of network-level traffic flow relationships: some simulation results. *Transp. Res. Rec.* 971, 121–130.
- Mariotte, G., Leclercq, L., 2019. Flow exchanges in multi-reservoir systems with spillbacks. *Transport. Res. Part B: Methodol.* 122, 327–349.
- Mariotte, G., Leclercq, L., Laval, J.A., 2017. Macroscopic urban dynamics: Analytical and numerical comparisons of existing models. *Transport. Res. Part B: Methodol.* 101, 245–267.
- Mascia, M., Hu, S., Han, K., North, R., Van Poppel, M., Theunis, J., Beckx, C., Litzenberger, M., 2017. Impact of traffic management on black carbon emissions: a microsimulation study. *Networks Spatial Econ.* 17 (1), 269–291.
- Mayne, D.Q., 2014. Model predictive control: Recent developments and future promise. *Automatica* 50 (12), 2967–2986.
- Ni, W., Cassidy, M., 2019. City-wide traffic control: modeling impacts of cordon queues. *Transport. Res. Part C: Emerg. Technol.*
- Ntziachristos, L., Gkatzoflias, D., Kouridis, C., Samaras, Z., 2009. COPERT: a european road transport emission inventory model. In: *Information technologies in environmental engineering*. Springer, pp. 491–504.
- Osorio, C., Nanduri, K., 2015. Urban transportation emissions mitigation: Coupling high-resolution vehicular emissions and traffic models for traffic signal optimization. *Transport. Res. Part B: Methodol.* 81, 520–538.
- Pasquale, C., Papamichail, I., Roncoli, C., Saccone, S., Siri, S., Papageorgiou, M., 2015. Two-class freeway traffic regulation to reduce congestion and emissions via nonlinear optimal control. *Transport. Res. Part C: Emerg. Technol.* 55, 85–99.
- Pasquale, C., Saccone, S., Siri, S., De Schutter, B., 2017. A multi-class model-based control scheme for reducing congestion and emissions in freeway networks by combining ramp metering and route guidance. *Transport. Res. Part C: Emerg. Technol.* 80, 384–408.
- Saedi, R., Verma, R., Zockaie, A., Ghamami, M., Gates, T., 2018. A framework for incorporating the network-wide fundamental diagram into large-scale emission estimation. *J. Transport & Health* 9, S54–S55.
- Samaras, Z., Tsokolis, D., Toffolo, S., Magra, G., Ntziachristos, L., Samaras, Z., 2019. Enhancing average speed emission models to account for congestion impacts in traffic network link-based simulations. *Transport. Res. Part D: Transp. Environ.* 75, 197–210.
- Shabihkhani, R., Gonzales, E., 2014. Macroscopic relationship between network-wide traffic emissions and fundamental properties of the network. *Transport. Res. Circular E-C197. Proc., Symposium Celebr.* 50, 284–299.
- Sirmatel, I.I., Geroliminis, N., 2016. Model predictive control of large-scale urban networks via perimeter control and route guidance actuation. In: *2016 IEEE 55th Conference on Decision and Control (CDC)*. IEEE, pp. 6765–6770.
- Sirmatel, I.I., Geroliminis, N., 2018. Economic model predictive control of large-scale urban road networks via perimeter control and regional route guidance. *IEEE Trans. Intell. Transp. Syst.* 19 (4), 1112–1121.
- Song, J., Hu, S., Han, K., Jiang, C., 2019. Nonlinear decision rule approach for real-time traffic signal control for congestion and emission reductions.
- Thaker, P., Gokhale, S., 2016. The impact of traffic-flow patterns on air quality in urban street canyons. *Environ. Pollut.* 208, 161–169.
- Wang, Y., Szeto, W., Han, K., Friesz, T.L., 2018. Dynamic traffic assignment: A review of the methodological advances for environmentally sustainable road transportation applications. *Transport. Res. Part B: Methodol.*
- Yang, K., Zheng, N., Menendez, M., 2017. Multi-scale perimeter control approach in a connected-vehicle environment. *Transport. Res. Part C: Emerg. Technol.*
- Ye, B.-L., Wu, W., Ruan, K., Li, L., Chen, T., Gao, H., Chen, Y., 2019. A survey of model predictive control methods for traffic signal control. *IEEE/CAA J. Autom. Sin.* 6 (3), 623–640.
- Yildirimoglu, M., Sirmatel, I.I., Geroliminis, N., 2018. Hierarchical control of heterogeneous large-scale urban road networks via path assignment and regional route guidance. *Transport. Res. Part B: Methodol.* 118, 106–123.
- Zegeye, S.K., De Schutter, B., Hellendoorn, H., Breunese, E., 2009. Reduction of travel times and traffic emissions using model predictive control. In: *2009 American Control Conference*. IEEE, pp. 5392–5397.